Spatial variability of air pollutants in a megacity characterized by mobile measurements~~: Chemical homogeneity under haze conditions~~

Reza Bashiri Khuzestani[1,2,†], Keren Liao[1,†], ~~Qi Chen[1,*],~~ Ying Liu[1], Ruqian Miao[1], Yan Zheng[1], Xi Cheng[1], Tianjiao Jia[1], Xin Li[1], Shiyi Chen[1], Guancong Huang[1], Qi Chen[1,*]

[1]State Key Joint Laboratory of Environmental Simulation and Pollution Control, BIC-ESAT and IJRC, College of Environmental Sciences and Engineering, Peking University, Beijing, 100871, China
[2]Now at: Faculty of Civil, Water and Environmental Engineering, School of Engineering, Shahid Beheshti University, Tehran, Iran
[†]Equal Contribution.

[*]*Correspondence to*: Qi Chen (qichenpku@pku.edu.cn)

Abstract. Characterization of the spatial distributions of air pollutants on an intracity scale is important for understanding local sources, secondary formation, and human exposure. In this study, we conducted in situ mobile measurements for the chemical composition of fine particles, volatile organic compounds (VOCs), oxygenated VOCs (OVOCs), and common gas pollutants in winter in the megacity of Beijing. The spatial ~~variations~~ patterns of these ~~gaseous and particulate~~ pollutants under different pollution conditions ~~are~~ were investigated. During the ~~less polluted periods~~non-haze days, all pollutants showed significant spatial variability. Large spatial variations of secondary species including OVOCs and secondary aerosol species highlight the chemical heterogeneity. In particular, ~~a large spatial variability exists in~~ the inorganic chemical ~~inorganic~~ composition of fine particles varied greatly on the 65-km urban highway, suggesting a wide range of particle neutralization in the megacity of Beijing. ~~Significant spatial variations are also observed in the composition of organic aerosol (OA), which are driven by primary OA emissions from vehicle and cooking exhaust as well as oxygenated OA~~Localized sources such as vehicle, cooking, and industry emissions led to hot spots and nonuniform distributions of primary pollutants in the city. ~~The spatial variations of VOCs and OVOCs vary by species. In general, hydrocarbon compounds show a large spatial variability that is attributed to traffic plumes, while secondary OVOCs are more spatially homogeneous in concentration because of the predominant contribution of urban background to the on-road air. Other gas pollutants show relatively low spatial variabilities and some high concentration spots that indicate high emitting plumes from local sources as well as fast on-road ozone titration.~~ The spatial heterogeneity of air pollutants under less-polluted conditions calls a future need of using fine-resolution models to evaluate human exposure and to develop pollution control strategies. During the haze ~~periods~~day, the spatial ~~variabilities~~ variabilities of ~~air~~ secondary gaseous and particulate pollutants~~pollutants~~ ~~are~~ were largely reduced, explained by both of the elevated urban background from polluted air mass and the enhanced secondary formation by elevated precursor concentrations and heterogeneous or aqueous pathways. Although localized primary emissions were accumulated under stagnant haze conditions, the chemical composition of fine particles became relatively homogeneous because of the predominant secondary contributions. An uniform spatial pattern of particle neutralization was observed. ~~because of the predominant contribution of~~

~~regional transport to the on-road concentrations of these pollutants.~~ The concentrations of hydrocarbons and less-oxygenated OVOCs show~~ed~~ good positive spatial-temporal correlations during the haze day, while~~. T~~ the concentrations of more-oxygenated OVOCs show~~ed~~ good positive correlations among themselves but moderate negative correlations with the concentrations of hydrocarbons, less-oxygenated OVOCs, and ~~particulate components~~aerosol species. ~~-~~Our results indicate a spatial chemical homogeneity on the megacity scale to promote~~The similar chemical compositions of particles and their gaseous precursors on the megacity scale suggest a spatially chemical homogeneity that may lead to~~ efficient SOA production under haze conditions. ~~On the other hand, the spatial heterogeneity of air pollution under less-polluted conditions calls a future need of using fine-resolution models to evaluate human exposure and pollution control strategies.~~

1 Introduction

Air quality degradation has become a serious problem in developing countries (Huang et al., 2014; Khuzestani et al., 2017). Cities in northern China suffer from severe haze events, especially in winter (Huang et al., 2014). High concentrations of volatile organic compounds (VOCs) and nitrogen oxides ($NO_x = NO + NO_2$) contribute to high atmospheric oxidation capacity to produce ozone (O_3) and secondary aerosol (Wang et al., 2017; Lu et al., 2019b). The mass concentrations of particles having aerodynamic diameter less than 2.5 μm ($PM_{2.5}$) may reach up to several hundreds of μg m^{-3}, and the O_3 concentrations may exceed 100 ppbv in megacities. Both of high exposures of $PM_{2.5}$ and O_3 are of great concern to human health (Liu et al., 2016; Bell et al., 2006).

Tremendous efforts have been made to characterize air pollutants in populated urban areas in China (Li et al., 2017; Wang et al., 2017; Quan and Jia, 2020). In most studies, stationary measurements were conducted to obtain the temporal variations of air pollutants for the analysis of their sources and formation mechanisms. Sulfate, nitrate, ammonium, and organic aerosol (OA) are the major chemical components of $PM_{2.5}$ in cities in China (Li et al., 2017). Their mass concentrations show decreases nationwide since 2013 as a result of the emission reduction of gaseous precursors such as sulfur dioxide (SO_2), NO_x, and VOCs under clean air actions as well as the changes of meteorological conditions (Zhang et al., 2019). ~~In Beijing, the contribution of secondary OA (SOA) has significantly increased since 2018, while the contribution of primary OA (POA) from burning of coal and biomass (biofuel) and cooking emissions have decreased.~~ Characterization of ~~organic precursors including~~ VOCs ~~and~~ as well as oxygenated VOCs (OVOCs) ~~semivolatile and intermediate volatility organic compounds (S/IVOCs)~~ is crucial for understanding the formation of O_3 and secondary OA (SOA) production. ~~Previous studies have shown that b~~Besides alkanes, aromatics and ~~oxygenated VOCs (~~OVOCs~~)~~ are abundant in ~~cities~~ urban areas in China (Mozaffar and Zhang, 2020; Li et al., 2016; Guo et al., 2017). These ~~VOCs~~organic compounds may come from a variety of anthropogenic sources ~~(e.g.,~~such as vehicles, industries, solvent usage, coal and biomass burning, and household use of volatile chemical products etc.~~) and have great potential to form O_3 and SOA.~~ In Beijing, the contribution of ~~secondary OA (~~SOA~~)~~ has significantly increased since 2018, while the contribution of primary OA (POA) from burning of coal and biomass (biofuel) and cooking emissions to $PM_{2.5}$ have decreased (Lei et al., 2021).

On an intracity scale, local emissions, advection, and boundary layer evolution ~~may~~ affect the spatial distributions of air pollutants. Tower measurements have shown greater vertical gradients of particulate matter (PM) concentration and composition during clean periods than haze periods in Beijing, which is attributed to the influence of both physical (e.g., regional transport, mixing layer height, and inversions etc.) and chemical processes (e.g., gas-particle partitioning and aqueous processing) (Zhou et al., 2018). The VOC concentrations also show ~~S~~significant vertical gradients ~~also present in the concentrations of VOCs~~ in cities, ~~which can be~~ affected by the transport of air mass, vertical diffusion, and species reactivity (Sun et al., 2018; Mo et al., 2020). ~~However, the spatial variability of air pollutants remains unclear, limiting our understanding of the haze development. Moreover, g~~Grid sampling and simultaneous measurements at multiple sites ~~are often used to~~

~~investigate the spatial variations of air pollutants on sparse spatial scales. Previous studies~~ have shown that the surface concentrations of VOCs and $PM_{2.5}$ chemical components can vary significantly on sparse spatial scales because of different source contributions in metropolitan areas in China (Chen et al., 2020; Song et al., 2021). Such measurements are however limited. The spatial variability of air pollutants remains quite unclear, limiting our understanding of source distribution, haze development, and human exposure. ~~However, the spatial variability of air pollutants remains unclear, limiting our understanding of the haze development.~~

~~To better characterize the spatial distributions of air pollutants, m~~Mobile laboratory equipped with fast response in situ instruments have been widely used in Europe and United States to better characterize the spatial distributions of air pollutants (Kolb et al., 2004). For example, mobile measurements in Pittsburgh and Zurich indicate different spatial variability of ~~PM~~ submicron particle composition (Tan et al., 2014; Gu et al., 2018; Ye et al., 2018; Mohr et al., 2011; Elser et al., 2016). While primary carbonaceous sources ~~perhaps~~ le~~a~~d to the large spatial heterogeneity of ~~PM~~ the particle composition in Pittsburgh, a rather uniform distribution was observed in the metropolitan area of Zurich especially during thermal inversions over the Swiss plateau~~, highlighting the complexity of urban air pollution~~. ~~However, the development and application of advanced mobile laboratory are lagged in China.~~ In China, ~~M~~mobile measurements have been conducted to obtain the spatial distributions of SO_2, NO_x, carbon monoxide (CO), and black carbon (BC) as well as the column densities of NO_2 and SO_2 ~~column densities~~ for the evaluation of regional transport routes in North China Plain (NCP) and the sources of ~~air~~ these pollutants (Wang et al., 2009; Wang et al., 2011; Zhu et al., 2016; Wu et al., 2018). ~~Recent deployments of o~~Online mass spectrometers ~~in mobile laboratory~~ for~~have successfully captured the spatial distributions of~~ VOCs and $PM_{2.5}$ chemical composition have also been used on the mobile measurements~~in cities in China~~, ~~which may be useful for further investigation of urban air pollutio~~although the~~n~~ spatial variabilities of these pollutants have not yet been systematically investigated (X. Wang et al., 2021; Liang et al., 2020; Liao et al., 2021).

In this study, we conducted in situ sampling with gas analyzers and ~~advanced~~ mass spectrometers on a newly developed mobile laboratory ~~platform~~ in winter in ~~the megacity of~~ Beijing. Spatial distributions of the mass concentrations of non-refractory $PM_{2.5}$ (NR-$PM_{2.5}$) components (i.e., OA, nitrate, sulfate, ammonium, and chloride), VOC and OVOC species, and common gas pollutants such as SO_2, CO, NO, NO_2, and O_3 ~~are~~ were obtained. The spatial variabilities of these gaseous and particulate pollutants under different pollution conditions ~~are~~ were investigated to provide new insights to understand ~~urban pollution and to improve our understanding of human exposure~~.

2 Methods

On-road measurements were conducted by the PKU mobile laboratory ~~(Figure S1 in the Supplement)~~ on the 4th Ring Road of Beijing on 7-21 November 2018. The 4th Ring Road is a 65-km-long urban highway that passes through ~~commercial, industrial, and~~ residential, commercial and services, park, and transportation areas in the megacity (Figure 1a). ~~To show the~~

~~spatial characteristics, the measurement area is categorized into 4 zones: Zone NE, Zone NW, Zone SE, and Zone SW (Figure S2 in the Supplement). Zone SE and Zone SW are close to i~~Industrial facilities~~, while Zone NE and Zone NW are mostly commercial and residential areas~~ are mostly located in the south of Beijing and outside of the 4th Ring Road. The average traffic volume on the 4th Ring Road is ~~about 4000–8000~~ about 1.2×10^4 vehicles per hour (Figure 1b), and over 90% of the fleet consisted of light duty gasoline vehicles (LDGVs) that meet National Stage III to V emission standards (Wu et al., 2017; Deng et al., 2020; Lv et al., 2020). ~~The~~ Our measurements started at around 9:00 a.m. and went one cycle after another till 4:00 p.m. to avoid rush hours. Each cycle took approximately 70 min with a mean speed of 60 km h^{-1}. Self-contamination from the vehicle exhaust should be ~~is~~ negligible for a vehicle speed over 30 km h^{-1} (Liao et al., 2021). The data that were collected at a speed of less than 30 km h^{-1} during occasional traffic jams have been excluded from the analysis.

A suite of instruments was deployed in the mobile laboratory. Detailed information about the ~~campaign, sampling system,~~ instrument operation, calibration, and data analysis are provided in Sect. A of the Supplement. Gas and particle inlets were installed at the top front of the vehicle (i.e., about 3.4 m above ground) to sample on-road air that was influenced by diluted vehicle exhaust (Figure S1 in the Supplement). Gas pollutants were detected by gas analyzers including NO_2 (Teledyne, T500U), NO-NO_x (Ecotech, EC9841A), SO_2 (Ecotech, EC9850A), CO (Ecotech, EC9830A), and O_3 (Ecotech, EC9810A) with a time resolution of 2 s. The chemical composition of NR-$PM_{2.5}$ was measured by an Aerodyne time-of-flight aerosol chemical speciation monitor (TOF-ACSM) equipped with $PM_{2.5}$ lens and ~~a~~ capture vaporizer. The time resolution was 40 s, corresponding to a spatial resolution of ~0.7 km for a driving speed of 60 km h^{-1}. The~~a~~ mass resolution was~~of~~ about 400. A collection efficiency of about unity was used, and the uncertainty of mass quantification was ~30% (Zheng et al., 2020). ~~The uncertainty for the mass concentrations of NR-$PM_{2.5}$ and its components is about 30%~~ (Canagaratna et al., 2007)~~. VOCs and OVOCs were detected by an Ionicon proton transfer reaction-quadrupole ion-guide time-of-flight mass spectrometer (PTR-QiTOF). The overall quantification uncertainties are <20% for calibrated species and 19% and 33% for uncalibrated species with known and unknown reaction rate constants (K_{ptr}), respectively~~ (Huang et al., 2019)~~. Table S1 in the Supplement lists the K_{ptr} values, the mean concentrations, and the tentative categorization of VOCs and OVOCs measured herein. Detailed information about the campaign, sampling system, instrument operation and calibration, and data analysis are provided in Sect. A of the Supplement.~~ The positive matrix factorization (PMF) analysis was performed on the unit-mass-resolution OA mass spectra for mass-to-charge ratio (m/z) of 12 to 200 by using the Igor PMF evaluation tool (PET, version 3.00B). Details are given in Table S1, Figures S2-S5, and Section A3 of the Supplement. A total ~~F~~of five OA factors ~~were~~ has been resolved including hydrocarbon-like OA (HOA), cooking-related OA (COA), and three oxygenated OA (OOAs). The common OA factors related to biomass burning (BBOA) or coal burning (CCOA) were not resolved in this data set ~~and were perhaps mixed with other OA factors~~ (Liao et al., 2021). Their contributions to OA were ~~however~~ expected to be small because of the stringent emission control in NCP in recent years (Zheng et al., 2020; Duan et al., 2020).

VOCs and OVOCs were detected by an Ionicon proton transfer reaction-quadrupole ion guide time-of-flight mass spectrometer (PTR-QiTOF) with a time resolution of 2 s. The overall quantification uncertainties ~~are~~ were less than 20% for calibrated

species, ~~and~~ and 19% ~~and~~ or 33% for uncalibrated species with known ~~and~~ or unknown reaction rate constants (K_{ptr}), respectively (Huang et al., 2019). Table S2 in the Supplement lists the K_{ptr} values, the mean concentrations, and the tentative categorization of VOCs and OVOCs measured herein (Yuan et al., 2017). A moving average window of 10 (i.e., 20 s) was applied to the entire data set for the VOC and OVOC species. Baseline concentrations for each 2-s point in the 20-s smoothed data ~~that represents~~ were calculated as the 5th percentile concentration within a rolling window of 60 (i.e., 120 s) to represent the well-mixed urban background ~~conditions~~. Figure S6 in the Supplement shows the time series and the baselines of selected VOC and OVOC concentrations during two typical runs on the 4th Ring Road. We computed the peak fraction (PF) parameter as 1 minus the ratio of the mean baseline value to the observed mean concentrations to indicate the contributions to the mean observed concentrations above the mean local baseline (Apte et al., 2017). In addition, we computed a batch of 12-hour backward trajectories for the height of 3 m around the 4th Ring Road from the Hybrid Single-Particle Lagrangian Integrated Trajectory (HYSPLIT) model to investigate the influence of regional transport on our measurements during the haze day (Stein et al., 2015). ~~We set t~~The start time of the trajectory analysis was set at 9:00 a.m.~~-~~, and the trajectory calculations were repeated ~~the trajectory calculations~~ every 1 hour until 4:00 p.m. (Figure S7 in the Supplement).

~~Figure S3 in the Supplement shows the time series of mass concentrations of air pollutants measured at the PKU campus roof site during the campaign. This site is located between the 4th and the 5th north Ring Roads, representing a typical urban environment in Beijing~~ (Cheng et al., 2021)~~. In this study, we classified clean (< 35 μg m^{-3}), haze (> 75 μg m^{-3}), and non-haze (< 75 μg m^{-3}) days based on the daily mean $PM_{2.5}$ mass concentrations for the measurements. Moreover, we computed a batch of 12-hour backward trajectories for the height of 3 m around the 4th Ring Road from the HYSPLIT model to investigate the influence of urban background and regional transport on our measurements during the haze day~~ (Stein et al., 2015)~~. We set the start time of the trajectory analysis at 9:00 a.m. and repeated the trajectory calculations every 1 hour until 4:00 p.m. (Figure S4 in the Supplement). In addition, a moving average window of 10 (i.e., 20 s) was applied to the entire data set for VOC and OVOC species. Concentration baselines for each 2-s point in the 20-s smoothed data were calculated as the 5th percentile concentration within a rolling window of 60 (i.e., 120 s), for which the urban background conditions were identified~~ (Apte et al., 2017)~~. We then computed the peak fraction (PF) parameter as 1 minus the ratio of the mean baseline value to the observed mean concentrations. The time series of the concentrations of common VOC and OVOC species shows significant plumes above the baseline for the on-road measurements (Figure S5 in the Supplement). PF values are used as a semi-quantitative indicator to show the contributions of the above baseline concentrations to the observed concentrations of VOCs and OVOCs, which may represent the intensity of transient emission from local sources (e.g., vehicle exhaust).~~

3 Results and Discussion

3.1 Spatial distributions and variability during the non-haze days~~of NR-$PM_{2.5}$ and its components~~

Figure S8 in the Supplement shows the time series of meteorological parameters and mass concentrations (or mixing ratios) of air pollutants measured at the PKU roof site during the mobile campaign. The roof site is located between the 4th and the 5th North Ring Roads at about 30 m above the ground, representing a typical urban background environment in Beijing (Zheng et al., 2021). We classified haze (≥ 75 μg m^{-3}) and non-haze (< 75 μg m^{-3}) days based on the daily mean $PM_{2.5}$ mass concentrations measured at the roof site. The mobile measurements covered from 9 a.m. to 4 p.m. for 8 non-haze days and 1 haze day. Apte et al. (2017) suggest that a small number of drive days (i.e., < 5 days) may result in a biased data set to represent the long-term spatial patterns. Although we have limited data (1 day) to represent the weekend or haze conditions, some of the key characteristics of air pollutants from the mobile measurements are consistent with previous understanding about weekend effects and haze evolution in Beijing (Table S3 in the Supplement). For instance, lower mass concentrations of aerosol species presented at weekend than on weekdays in winter, similar to previous findings (Sun et al., 2015). NO_x and VOC concentrations were lower at weekend than on weekdays perhaps because of heavier traffic loads and anthropogenic activities. By contrast, O_3 concentrations were greater at weekend, indicating enhanced photochemical production (Wang et al., 2014; Liu et al., 2020). The severe haze event occurred on 13-14 November 2018 under stagnant weather conditions with occasional shifts between northerly and southerly winds (Figure S8). The $PM_{2.5}$ concentrations increased rapidly to nearly 300 μg m^{-3} during the event. Relative humidity (RH) increased and remained above 70% on 14 November 2018, which was often observed in the later stage of severe winter haze in NCP in China (Sun et al., 2016). The elevated RH can lead to a large increase of aerosol liquid water content which may promote aqueous or heterogeneous chemistry to enhance the formation of secondary species (Peng et al., 2021). Indeed, the mass concentrations of sulfate, nitrate, and OA increased greatly, and nitrate became the most abundant component during the haze day. Moreover, the meteorological conditions and pollutant concentrations were similar to previous findings in Beijing (Zheng et al., 2021). The aerosol compositions measured by the mobile laboratory within a distance of 1.5 km from the site were also similar to the roof-site observations (Figure 1c-d), taking into account the potential difference between PM_1 and $PM_{2.5}$ (Sun et al., 2020).

Figure 2~~3~~ shows the spatial distributions of the mean mixing ratios of gaseous pollutants~~ for the example noon cycles. The concentrations of SO_2 are low (< 10 ppbv) throughout the campaign (Figure 3a).~~ During the ~~clean day~~non-haze days, gas pollutants all showed significant spatial variability. The mean mixing ratios varied by 2-3 times for SO_2, CO, NO, NO_2, and O_3 and by 4 to 21 times for VOC subgroups on the 4th Ring Road. For SO_2, ~~t~~the mean mixing ratios~~he SO_2 concentrations~~ ranged from 3.7 to 7.1 ppbv~~are low in the north and relatively high in the west of the 4th Ring Road, which is different from the distributions of the NR-$PM_{2.5}$ mass concentrations.~~ The lack of hot spots in the spatial pattern indicates a minor influence of on-road or near-road (e.g., off-road engines) sources. The overall l~~The SO_2 concentrations has a CV of 0.13. The low spatial variability~~ow concentrations of SO_2 ~~may~~are consistent with the predominant contribution of regional transport as a result of the phasing out of coal use in Beijing including power plants, coal boilers, and residential stoves (Zheng et al., 2018; Ge et al., 2018)~~ be explained by the predominant contribution of regional transport as a result of the relocation of steel industry and~~

power plants out of Beijing and the ban of high-emission vehicles from the road. High SO_2 concentrations presented in the northwest segment, while the low concentrations were in the north segment. In summer, the southeast p Previous mobile measurementsrevailing wind can lead to higher concentrations of SO_2 in the southeast and lowest areas in Beijing captured specific transport events of SO_2 from the south and found that the SO_2 concentration decreased from Zone SE to Zone NW (Wang et al., 2011; Zhu et al., 2016)., which is consistent with our clean-day observations. The northwest prevailing wind in winter is however considered as clean air mass away from the NCP regional sources (Figure 1c). The relatively high SO_2 mixing ratios in the northwest segment may be associated with residential coal burning near the mountain area where the replacement of coal has been lagged compared with the plain area.

For CO, CO and NO are common gaseous pollutants emitted from combustion sources. Tthe mean mean on-road concentrationsmixing ratio of 1.5 ± 0.7 o ppmvf CO are 1.53 ± 0.66 ppm for non-haze days. For comparison, the concentrations of CO measured concurrently at the PKU roof site are 0.50 ± 0.26 ppm for non-haze days. The on-road concentrations arewas about three times greater than the urban background level concentrations (0.5 ± 0.3 ppm at the PKU roof site), , explained by the contribution ofindicating significant contributions of vehicle exhaustlocalized sources during the non-haze days plumes . For NO, the concentrations measured at the PKU roof site are very low because of the O_3 titration. The on-road concentrations are 1-2 orders of magnitude greater, which is also explained by the fleet emissions. The clean-day spatial distribution of CO concentrations (CV = 0.26) is quite homogeneous except a few hot spots in Zone SW (Figure 3b). The clean-day spatial distribution of NO concentrations (CV = 0.22) is different from that of CO (Figure 3c), showing higher concentrations in Vehicle emissions are Zone SE where the traffic volume is usually greater than in other Zones. One explanation for such differences between CO and NO may be much greater contributions of background concentrations and non-vehicular sources to CO. the main local source of NO_x and CO in Beijing (Qi et al., 2017). The spatial distribution of NO_x was generally consistent with that of CO, showing relatively high mixing ratios in the west and east segments of the 4th Ring Road (Figure S9 in the Supplement). Differences remained in the southwest corner where CO showed high concentrations but NO_x did not, which was perhaps related to non-vehicle sources or different fleet composition. In addition, relatively slower response of instrument detection of CO and NO may smooth out some of the concentration variations. As shown in Fig. S6 in the Supplement, the on-road time series of NO_2 concentrations shows more short-duration peaks than the time series of CO and NO concentrations.The clean-day spatial distribution of NO_2 concentrations is similar to that of NO, although more concentration hot spots exist (Figure 3d). The on-road On-road NO_2 arecan be contributed by direct tailpipe NO_2 emissions, secondary NO_2 through on-road NO_x titration, and urban background NO_2. T The tailpipe NO_2 emissions are small for LDGVs (of National Stage III are and above) very low (Wu et al., 2017). The urban background concentrations of NO_2 measured at the PKU roof site on 18 November 2018 (clean day) are low at noon (5.2 ± 0.6 ppbv). T The high mixing ratios of on-road high on-road NO_2 concentrations (102.9 ± 37.3 ppbv16.8-94 ppbv) indicate are plausibly contributed by strong on-road the fast on-road NO_x titration of NO_x, which is similar to the findings in North Carolina, U.S. (Yang et al., 2018), comparing with the low urban background level (23.0 ± 14.4 ppbv at the roof site). As shown in Fig. S7a in the Supplement, In winter, the site

was located in the upwind direction and was less affected by urban traffic emissions during the non-haze days. Because of the fast on-road titration, ~~the clean-day on-road concentrations of O_3 range from 3.2 to 15.4 ppbv, which are 3–4 times lower than the concentrations measured at the PKU roof site (40.0–44.5 ppbv). T~~the spatial ~~distribution~~ patterns for ~~of~~ O_3 ~~concentration~~ ~~is~~and NO were anti-correlated (Pearson r = -0.43) ~~opposite to that of NO, which is consistent with the titration effect~~ and~~,~~ ~~The more frequent appearance of hot spots in the clean-day NO_2 distribution is likely because of the faster detection of NO_2 by the cavity-attenuated phase-shift technique than the chemiluminescence detection of NO.~~ the mean mixing ratio of on-road O_3 (11.2 ± 2.2 ppbv) were over 2 times lower than the roof-site observations (25.7 ± 12.8 ppbv). Overall, the spatial pattern of NO_x was consistent with the bottom-up emission inventory for (1) the nonuniform vehicle emissions on the 4th Ring Road and (2) high concentrations in the east segment of the 4th Ring Road where the traffic volume was high (Figure 1b and Figure S10 in the Supplement).

The spatial distributions of VOCs varied~~y~~ by species. LDGVs emit aromatic hydrocarbons (e.g., benzene, toluene, ethylbenzene, and xylenes) and~~,~~ some oxygenated species (e.g., acetaldehyde)~~, and so on~~ (Gentner et al., 2017). As expected, the on-road concentrations of such primary VOCs ~~species are~~ were much greater than the concentrations measured at the urban and suburban sites in Beijing (Table S1~~2 in the Supplement~~). ~~Figure 3e–f shows the spatial distributions of benzene and toluene concentrations.~~ During the ~~clean day~~non-haze days, the tentatively-assigned group of ~~both of the~~ acids/anhydrides showed the greatest spatial variability (by 21×), while the groups of hydrocarbons and aldehydes/ketones showed less variability (by 4× and 9×, respectively) (Table S2)~~distributions show large spatial variabilities with high CV values (Table 1)~~. While hydrocarbons were affected by localized sources such as vehicles, solvent use, and possibly some solid-fuel combustion in the mountain area (L. W. Wang et al., 2021), the strong spatial variability of acids/anhydrides can be explained by their secondary nature, meaning that the photochemical production depends on the precursor and oxidant level and can be spatially heterogeneous. Aldehydes/ketones may have both primary and secondary sources and showed greater spatial variability than hydrocarbons. The toluene-to-benzene concentration ratio (T/B) has been widely used to differentiate the VOC sources. Some hot spots in the spatial pattern of hydrocarbons (e.g., high concentrations in the northwest corner and the northeast segment) were plausibly contributed by transient plumes of vehicle exhaust (Figure S10). The T/B ratios was ~1 in the northwest corner and ~2 in the northeast segment (Figure S9), suggesting perhaps different fleet composition (Mo et al., 2016). Some other high T/B ratios (~3) in the south and southeast segments might be affected by industry emissions in the south of Beijing (Figure 1a). Industry and solvent emissions have greater T/B ratio than vehicle emissions, whereas emissions from biomass or solid fuel burning or aged air mass typically have lower T/B ratios (Song et al., 2021; and references therein). The spatial patterns of hydrocarbons (or benzene and toluene) were different from that of NO or NO_x, explained by the potential differences in fleet composition and urban background contributions as well as the chemical conversion rate.

~~Concentration hot spots present and are plausibly contributed by transient plumes of vehicle exhaust or nearby local sources (e.g., in industrial areas of Zone SW). Interestingly, the distributions of the hot spots for benzene and toluene are not the same, highlighting the difference in emissions from individual vehicles . The toluene-to-benzene concentration ratio (T/B) is widely~~

~~used to differentiate the VOC sources . According to literature, traffic emissions have T/B ratios from 1 to 3 depending on vehicle type and fuel composition. Industry emissions have a wide range of T/B ratios (1.4 to 5.8). Solvent emissions may have high T/B ratio of ~ 8.8. Biomass burning emissions typically have a low ratio of ~ 0.3. During the clean day, most of the concentration hot spots for benzene and toluene corresponds to T/B ratios of 1.1-2.6, which is consistent with vehicle emissions (Fig. S7b in the Supplement). Some of the high T/B ratios (e.g., 2-3 in the south) are perhaps related to industry plumes. The T/B ratios for on-road background (not high emitting plumes) are low (0.6-1.3), which may be explained by faster photochemical consumption of toluene than benzene. By contrast, the spatial variability for OVOCs (CV ~ 0.6) is much lower than that for hydrocarbons (Table 1), owing to their secondary nature because of the lack of local sources in Beijing .~~

Figure 3 shows the spatial distributions of the mean mass concentrations of key $PM_{2.5}$ components. During the non-haze days, the mean concentrations of OA, nitrate, sulfate, and ammonium on the 4th Ring Road varied by ~~9~~6 to 13~~+~~ times~~s~~. The ~~Significant spatial variabilities of the mass concentrations of NR-$PM_{2.5}$ and its chemical components are observed during the campaign. As described briefly by~~ Liao et al. (2021)~~, the mean (± one standard deviation) mass concentration of NR-$PM_{2.5}$ for non-haze days is 30.7 ± 24.7 μg m^{-3}, in which OA is the most abundant component that contributes to about 52% of the NR-$PM_{2.5}$ mass. The mean mass concentration of NR-$PM_{2.5}$ for the haze day is 155.0 ± 27.0 μg m^{-3}, and nitrate becomes the most abundant component that contributes to about 48%. Interestingly, the intracity spatial variations of the concentration and composition of NR-$PM_{2.5}$ are quite different under different pollution conditions.~~

~~Figure 1 shows the spatial distributions of the mass concentrations of organic and inorganic components in NR-$PM_{2.5}$ for the example noon cycles on typical clean and haze days.~~ coefficients of variation (CV, the standard deviation divided by the mean) of the four components and chloride ranged from 38% to 84%, indicating strong variability on the 24×17 km intracity scale (Table S4 in the Supplement)~~The coefficients of variation (CV) are listed in Table 1. Large spatial variabilities of the mass concentration and the composition of NR-$PM_{2.5}$ present in the clean-day measurements (Figure 1a)~~. The spatial variability of aerosol species was similar to that of VOCs but greater than that of other gas pollutants. ~~The mass concentration of NR-$PM_{2.5}$ ranges from 1.0 to 17 μg m^{-3} with a relatively high CV value of 0.75.~~ OA was the ~~dominant~~ major ~~component~~ contributor to the NR-$PM_{2.5}$ mass ~~(CV = 0.75)~~ (Table S3). Its concentration varied by 9 times on the 4th Ring Road~~(Table S3)~~. The spatial variability of the OA mass was attributed to both of POA and S~~O~~OA. As shown in Figure ~~3~~4, the mass concentrations of POA factors such as HOA and COA varied from 0 to 20 μg m^{-3} with hot spots in different segments of the 4th Ring Road. The 40-s $PM_{2.5}$ measurements by TOF-ACSM may roughly represent a maximum area of 0.16 km^2 (for a mean speed of 6 m s^{-1} and wind direction perpendicular to the mobile path) upwind when the mobile laboratory was run on the 4th Ring Road by cycles. ~~These hot spots might be explained by exhaust plumes from on-road vehicles and nearby restaurants that have not yet well mixed with urban background air.~~The HOA hot spots are generally consistent with the locations where the traffic volume was high and the driving speed was relatively low (Figure S10 of the Supplement). The COA hot spots are consistent with the places where the 4th Ring Road passes through sparsely located residential areas (Figure 1a). Moreover, the mass concentrations of the sum of OOAs varied from 0 to 15 μg m^{-3}. Local photochemical production of SOA is a significant source

of OA in Beijing in winter, although the solar radiation is reduced (Duan et al., 2020; Lu et al., 2019a). The photochemical production depends on the distributions of SOA precursors and oxidants. In the northwest corner where hydrocarbons showed high concentrations, the OOA mass loadings were indeed high. Because the majority of the SOA precursors (i.e., intermediate volatility and semivolatile organic species from anthropogenic sources) were not measured by the PTR-Qi-ToF (Liao et al., 2021; Miao et al., 2021), it is difficult to investigate more about the OOA source. ~~Similarly, t~~The measurements in Pittsburgh also showed a significant spatial heterogeneity of primary carbonaceous components such as HOA, COA, and BC (Gu et al., 2018). ~~The Pittsburgh study show l~~Less spatial ~~variabilities~~ variability~~of~~ presented for OOAs in the Pittsburgh study~~s, whereas the CV value for the OOA concentration are high in Beijing during the clean day~~. ~~This is perhaps because the precursors and formation pathways of OOAs are more complicated in Beijing than in Pittsburgh~~The OA mass loadings in Pittsburgh were however much less than the loadings in Beijing. The SOA formation can be significantly more efficient and complicated under conditions of high oxidative capacity and abundant precursors in Beijing than in Pittsburgh (Lu et al., 2019a; Li et al., 2021; Yang et al., 2019). Non-perfect separation of POA and SOA by the PMF analysis may also lead to misplaced spatial variability in OOA (Section A3).

Among the i~~I~~norganic ~~components~~ aerosol species, chloride has the highest CV ~~show much higher CV values in mass fraction than OA~~(Table S4). The mean concentration of chloride varied from below detection limit (0.04 μg m^{-3}) to 0.6 μg m^{-3} ~~(Table 1), indicating a relatively greater spatial variability of inorganic composition. As shown in Fig. 1b, ammonium is the predominant inorganic component in Zones NW and SW, while nitrate contributes most in Zone SE. The~~ . Although the TOF-ACSM equipped with capture vaporizer may underestimate the chloride mass concentrations by a factor of 2, its contribution to the mass and spatial variability of $PM_{2.5}$ were negligible. The main source of chloride in winter in Beijing is coal burning by regional transport, which should not lead to high spatial variability. The cause of such a high spatial variability of chloride during the non-haze days remains unknown. One hypothesis is the resuspended particles from the road (Chen et al., 2012). The spatial variability of sulfate, nitrate, and ammonium were similar in terms of CV and the concentration variations. The spatial pattern of ammonium however showed a large heterogeneity. ~~CV values for ammonium are the highest in both mass concentration and mass fraction.~~ The molar ratio of $n_{NH_4^+}$: ($2\times n_{SO_4^{2-}} + n_{NO_3^-}$) ranged from ~ ~~0~~0.5 to 1.~~0~~7 (Figure 5), suggesting a wide range of particle neutralization ~~on the megacity scale under clean day conditions~~ in winter in Beijing during the non-haze days. ~~, which is perhaps driven by the difference in chemical processes and local emissions of precursors.~~ In ~~NCP~~Beijing, the aerosol mass can be sensitive to either ammonia or the ~~nitric acid~~ availability of nitric acid (Nenes et al., 2020). Traffic and agriculture (e.g., livestock) emissions are the main sources of ammonia in Beijing ~~during the clean periods~~ in winter (Sun et al., 2017; Pan et al., 2018). ~~Traffic emissions~~The former depends on ~~on-road~~ vehicle type and volume and hence may vary greater on the Ring Road ~~greatly~~(Sun et al., 2017) ~~in the city~~. ~~On the other hand, t~~The concentrations of nitric acid depend on the concentrations of NO_x and hydroxyl radical (OH), which ~~that are affected by local emissions and atmospheric oxidation and may~~ may also ~~also~~ vary ~~significantly in the city~~spatially. ~~Besides, a~~Besides, the ~~uniform~~ distribution of solar radiation on the surface ~~is not expected in the megacity~~is nonuniform because of the shades of buildings ~~as well as~~and occasional cloud

covers. Therefore, the spatial heterogeneity of inorganic composition reflects spatiallycan be caused by different thermodynamic regimes in the megacity environment, which may challenge the development of further pollution control strategies as clean air actions continue. For comparison, tThe inorganic components composition have less spatial variabilities variability in Pittsburgh than in Beijing (Gu et al., 2018). A possible explanation is that the formation of ammonium nitrate is sensitive to ammonia only in Pittsburgh (Nenes et al., 2020), which may be explained by the greater emissions of ammonia and NO_x as well as OH concentrations in urban areas in China. The heterogeneity of inorganic composition can be seen in each of the single cycle on the 4th Ring Road (Figure S11 in the Supplement).

By contrast, the mass concentration of NR-$PM_{2.5}$ has a low CV value of 0.12, and it is consistently higher in Zones NE and NW (163.2 ± 12.3 μg m^{-3}) than in Zones SE and SW (138.8 ± 16.9 μg m^{-3}) during the haze day (Figure 1d). The mass fractions of inorganic (i.e., ammonium, sulfate, nitrate, chloride) and organic components (i.e., HOA, COA, and OOA) are similar across the city (CV < 0.35), although a few hot spots of COA exist (Figure 1f). The sampling inlets of the PKU mobile lab are located at 3.4 m above the ground, which may sample air from both of urban background and instantaneous plumes. The 40-s $PM_{2.5}$ measurements by TOF-ACSM may roughly represent a maximum area of 0.16 km^2 upwind when the mobile laboratory was run on the 4th Ring Road by cycles. The similar chemical composition along the road suggests relatively homogeneous spatial distributions of the mass concentration and composition of NR-$PM_{2.5}$ across the city under haze conditions. This is supported by the fact that the particle composition observed at the PKU roof site was similar to our mobile measurements (Figure S3). Although stagnant conditions facilitate the accumulation of local emissions (e.g., vehicle emissions on the road), over 60% of the $PM_{2.5}$ mass in Beijing can be contributed by regional transport during the winter haze episodes (Sun et al., 2014; Wu et al., 2021). The predominant contribution of regional transport suggests similar sources of $PM_{2.5}$ in Beijing. Similar particle composition suggests a spatial chemical homogeneity at least on the megacity scale in terms of gas-to-particle equilibrium or partitioning as well as the heterogeneous or particle-phase production. The north-south difference in mass concentration is perhaps driven by the differences in atmospheric dilution on the intracity scale (Sun et al., 2016; Chen et al., 2020). The uniform spatial distributions of PM composition under haze conditions are similar to the observations in the metropolitan area of Zurich when thermal inversions occur over the Swiss plateau and secondary pollution is built up regionally (Mohr et al., 2011), highlighting stagnant metrological conditions as one of the key drivers of the city-scale chemical homogeneity. Interestingly, the intracity spatial variations of the concentration and composition of NR-$PM_{2.5}$ are quite different under different pollution conditions.

Figure 2 shows the CV values of the mass fractions of ammonium, sulfate, nitrate, and OA in $PM_{2.5}$ for all cycles measured during the mobile campaign. Large spatial variabilities of the mass concentration and composition of NR-$PM_{2.5}$ present in all measurement cycles during the clean days, while the mass concentration and composition of NR-$PM_{2.5}$ are rather uniform in all cycles during the haze days on the 4th Ring Road, not limited to the noon cycle presented in Figure 1. The mass concentration and composition of NR-$PM_{2.5}$ show significantly day-to-day and diurnal variations as indicated by the stationary

~~measurements at the PKU roof site (Figure S3). Such temporal variations are driven by source variations and meteorological conditions, which have been studied extensively in the past~~ (Duan et al., 2020; Lei et al., 2021; and the reference therein)~~.~~ **3.2 Spatial distribution and variability during the haze day**

The spatial patterns of air pollutants were very different under different pollution conditions. As shown in Figure 2,

~~Figure 3 shows the spatial distributions of the mixing ratios of gaseous pollutants for the example noon cycles. The concentrations of SO_2 are low (< 10 ppbv) throughout the campaign (Figure 3a). During the clean day, the SO_2 concentrations are low in the north and relatively high in the west of the 4th Ring Road, which is different from the distributions of the NR-$PM_{2.5}$ mass concentrations. The SO_2 concentrations has a CV of 0.13. The low spatial variability of SO_2 may be explained by the predominant contribution of regional transport as a result of the relocation of steel industry and power plants out of Beijing and the ban of high-emission vehicles from the road~~ (Ge et al., 2018)~~. Previous mobile measurements in Beijing captured specific transport events of SO_2 from the south and found that the SO_2 concentration decreased from Zone SE to Zone NW~~ (Wang et al., 2011; Zhu et al., 2016)~~, which is consistent with our clean-day observations.~~ During the haze day,~~ the mean mixing ratios of SO_2 during the haze day ~~concentrations~~ were~~are~~ lower than t~~he concentrations observed during the~~he non-haze~~clean~~ -day case (Table S3), ~~which may be~~ explained by the large conversion of gaseous SO_2 to sulfate by both of the photochemical and aqueous processes under severe ~~winter~~ haze conditions (W. G. Wang et al., 2021). The mean mixing ratios of CO were however greater than the non-haze day ratios, indicating accumulated pollution. ~~The haze-day distribution of SO_2 concentration is different from the clean-day distribution and has a greater CV value of 0.27~~CO and SO_2 show relatively high concentrations in the east and north segments of the 4th Ring Road during the haze day. The haze in NCP is usually developed regionally, meaning that the polluted air mass travels and becomes more polluted when it stays in a place to accumulate local emissions and secondary production under stagnant conditions. The 12-hour backward trajectories around the 4th Ring Road show that the air masses were mostly from the east in the morning, started shifting towards south at ~12:00 p.m., and then were mainly originated from the south around 4:00 p.m. (Figure ~~S4~~ S7 in the Supplement). ~~The spatial distribution of SO_2 is therefore affected by the transport routes.~~ Southwesterly, southeasterly, and easterly fluxes ~~pathways~~ have been recognized as ~~typical regional transport routes~~regional pollution sources to Beijing (Chang et al., 2019). The spatial patterns of SO_2 and CO are thus consistent with the transport routes, and the low concentrations in the southwest suggest a possible edge of the polluted air mass (Peng et al., 2021). For NO, the mean mixing ratio at the PKU roof site during the haze day (46.0 ± 19.8 ppbv) was much greater than that observed for the non-haze days (14.7 ± 17.4 ppbv), but was still much lower than the on-road mixing ratios because of the titration.

~~CO and NO are common gaseous pollutants emitted from combustion sources. The mean on-road concentrations of CO are 1.53 ± 0.66 ppm for non-haze days. For comparison, the concentrations of CO measured concurrently at the PKU roof site are 0.50 ± 0.26 ppm for non-haze days. The on-road concentrations are about three times greater than the urban background concentrations, explained by the contribution of vehicle exhaust plumes~~ (Gentner et al., 2017)~~. For NO, the concentrations measured at the PKU roof site are very low because of the O_3 titration. The on-road concentrations are 1-2 orders of magnitude~~

~~greater, which is also explained by the fleet emissions. The clean-day spatial distribution of CO concentrations (CV = 0.26) is quite homogeneous except a few hot spots in Zone SW (Figure 3b). The clean-day spatial distribution of NO concentrations (CV = 0.22) is different from that of CO (Figure 3c), showing higher concentrations in Zone SE where the traffic volume is usually greater than in other Zones. One explanation for such differences between CO and NO may be much greater contributions of background concentrations and non-vehicular sources to CO. In addition, relatively slower response of instrument detection of CO and NO may smooth out some of the concentration variations. As shown in Fig. S6 in the Supplement, the on-road time series of NO_2 concentrations shows more short-duration peaks than the time series of CO and NO concentrations. During the haze day, greater CO and NO concentrations present. The spatial distributions of CO, NO, SO_2, and NR-$PM_{2.5}$ concentrations all show relatively low concentrations in Zone SW. The greater haze-day concentrations and the similar spatial distributions of these pollutants are consistent with the large contribution of regional transport to urban air pollution and the stagnant meteorological condition during the haze episode.~~

~~The clean-day spatial distribution of NO_2 concentrations is similar to that of NO, although more concentration hot spots exist (Figure 3d). The on-road NO_2 are contributed by direct tailpipe NO_2 emissions, secondary NO_2 through on-road NO_x titration, and background NO_2. The tailpipe NO_2 emissions are small for LDGVs (National Stage III and above)~~ (Wu et al., 2017)~~. The urban background concentrations of NO_2 measured at the PKU roof site on 18 November 2018 (clean day) are low at noon (5.2 ± 0.6 ppbv). The high on-road NO_2 concentrations (16.8-94 ppbv) are plausibly contributed by the fast on-road NO_x titration, which is similar to the findings in North Carolina, U.S.~~ (Yang et al., 2018)~~. As shown in Fig. S7a in the Supplement, the clean-day on-road concentrations of O_3 range from 3.2 to 15.4 ppbv, which are 3-4 times lower than the concentrations measured at the PKU roof site (40.0-44.5 ppbv). The spatial distribution of O_3 concentration is opposite to that of NO, which is consistent with the titration effect. The more-frequent appearance of hot spots in the clean-day NO_2 distribution is likely because of the faster detection of NO_2 by the cavity attenuated phase shift technique than the chemiluminescence detection of NO.~~ ~~During the haze day~~The spatial patterns of NO were similar for the non-haze and haze days, except the slightly greater concentrations in the north segment during the haze day.~~, the spatial distribution of O_3 concentration is opposite to that of NO but shows much lower concentrations (i.e., a few ppbv) than during the clean day, which can be explained by the stronger titration effect with higher NO concentrations. However, the concentrations of NO, NO_2, and O_3 are all high in Zone NW. The backward trajectories suggest transport of air masses from the east and the south to Beijing. The high concentrations of air pollutants in Zone NW therefore may not be explained by regional transport and are perhaps related to local meteorological conditions affected by specific land surface conditions.~~The mean NO_2 concentrations (69.7 ± 26.5 ppbv) were lower during the haze day than during the non-haze days (102.9 ± 37.3 ppbv). The corresponding PKU roof-site mean concentrations of NO_2 was 63.0 ± 8.8 ppbv, which is similar to the on-road concentrations. This indicates a potentially high urban background contribution to on-road NO_2 concentrations during the haze day, which is plausibly greater than its contribution during the non-haze days. The spatial pattern of NO_2 was determined by both on-road titration and urban background (similarly for O_3) during the haze day, and thus the spatial patterns of NO_2 and O_3 were different from those for the non-haze days.

Overall, the spatial variabilities for SO_2, CO, NO, NO_2, and O_3 were similar during the non-haze and haze days (i.e., varied by 2-4× with similar CV values) (Table S4). The spatial variability for VOCs was greatly reduced during the haze day (by 2-3× in contrast to 4-21× during the non-haze days), especially for the OVOCs.

~~The spatial distributions of VOCs vary by species. LDGVs emit aromatic hydrocarbons (e.g., benzene, toluene, ethylbenzene, and xylenes), some oxygenated species (e.g., acetaldehyde), and so on (Gentner et al., 2017). As expected, the on-road concentrations of such primary VOC species are much greater than the concentrations measured at the urban and suburban sites in Beijing (Table S1 in the Supplement). Figure 3e-f shows the spatial distributions of benzene and toluene concentrations. During the clean day, both of the distributions show large spatial variabilities with high CV values (Table 1). Concentration hot spots present and are plausibly contributed by transient plumes of vehicle exhaust or nearby local sources (e.g., in industrial areas of Zone SW). Interestingly, the distributions of the hot spots for benzene and toluene are not the same, highlighting the difference in emissions from individual vehicles (Mo et al., 2016).~~

~~The toluene-to-benzene concentration ratio (T/B) is widely used to differentiate the VOC sources (Song et al., 2021; and references therein). According to literature, traffic emissions have T/B ratios from 1 to 3 depending on vehicle type and fuel composition. Industry emissions have a wide range of T/B ratios (1.4 to 5.8). Solvent emissions may have high T/B ratio of ~ 8.8. Biomass burning emissions typically have a low ratio of ~ 0.3. During the clean day, most of the concentration hot spots for benzene and toluene corresponds to T/B ratios of 1.1-2.6, which is consistent with vehicle emissions (Fig. S7b in the Supplement). Some of the high T/B ratios (e.g., 2-3 in the south) are perhaps related to industry plumes. The T/B ratios for on-road background (not high-emitting plumes) are low (0.6-1.3), which may be explained by faster photochemical consumption of toluene than benzene. By contrast, the spatial variability for OVOCs (CV ~ 0.6) is much lower than that for hydrocarbons (Table 1), owing to their secondary nature because of the lack of local sources in Beijing (L. W. Wang et al., 2021).~~

~~During the haze day, a remarkable enhancement of VOC concentrations is observed with mean enhancement ratios of 3.3-16.3 (e.g., 8.7 for benzene, 6.5 for toluene, 6.5 for C_8 aromatics, 5.2 for methyl ethyl ketone, and 4.8 for propene) (Figure S8 in the Supplement).~~ The spatial ~~distributions~~ patterns of benzene and toluene during the haze day were different from those during the non-haze days with ~~show consistent high concentrations in Zones NW, SW, and SE (Figure 3e-f) but~~ lower T/B ratios. The low ratios suggest ~~in those segments that indicate~~ aged air mass during the haze day, which is consistent with the regional transport by polluted air mass ~~es~~ (de Gouw et al., 2005)~~, considering the limited biomass burning contributions during the campaign (Fig. S7b)~~. ~~The spatial distributions of benzene and toluene are different from the distributions of other air pollutants under haze conditions, suggesting that the influence of regional transport may vary by species. Moreover, the haze-day spatial distributions of OVOC concentrations are quite homogeneous with relatively small CV values (i.e., 0.14 for Σ (Aldehyde & Ketones) and Σ (Acids & Anhydrides) in Table 1).~~ The spatial patterns ~~distribution~~ of ~~individual~~ OVOC~~s~~s ~~is~~ are similar ~~among species~~to each other except for the OVOCs having 3-4 oxygen atoms in their formulae~~, which will be discussed~~(see more discussion ~~further~~ in Section~~.~~ 3.3). ~~The calculated PF values in Figure 4 suggest 30-40% contributions of high-emitting plumes to the on-road concentrations of aromatic species during the clean day compared with 9-13% during the haze day. For OVOCs~~

~~(e.g., formic acid), the contribution of high-emitting plumes to the on-road concentrations are comparable for the clean and haze days (i.e., 6-13%), owing to their secondary nature.~~The calculated PF for VOCs ranged from 11-67% (median) (Figure 6). High PF values were found for hydrocarbons and some OVOCs (e.g., C_8H_8, $C_{10}H_8$ and C_4H_4O), indicating a major contribution of transient localized sources (e.g., traffic, industrial facilities) to these species. The time series of these so-called primary species showed low baselines and sharp peaks (Figure S6). By contrast, OVOCs (i.e., with 2 or more oxygen in their formulae) that were typically considered as secondary species had low PF values (median: 11-16%) and elevated baseline contribution from photochemistry. Significance tests indicate greater PF values for the primary species during the non-haze days, meaning that the localized sources contributed more to the measured concentrations during the non-haze days than during the haze day ($p < 0.001$). During the haze day, the localized emissions should be accumulated near the source under stagnant conditions. Indeed, the peak concentrations of primary VOC species were significantly greater (e.g., ~2-4× for C_6H_6 and C_7H_8) (Figure S6). The lower PF values (by 30% for C_6H_6 and C_7H_8) during the haze day were caused by much more elevated baselines (e.g., ~9× for C_6H_6 and C_7H_8) that represent urban background affected by polluted air mass from regional transport plus gradually mixed local emissions. The mean VOC concentrations at the PKU roof site increased for about 2 times during the haze day, which agrees with the elevated baselines (Table S3 and Figure S12 in the Supplement).

~~By contrast, the mass concentration of NR-$PM_{2.5}$ has a low CV value of 0.12, and it is consistently higher in Zones NE and NW (163.2 ± 12.3 μg m^{-3}) than in Zones SE and SW (138.8 ± 16.9 μg m^{-3}) during the haze day (Figure 1d).~~ The haze-day mean concentrations of~~The mass fraction~~ aerosol species increased by about 5 times on the 4th Ring Road (Figure 3). ~~s of~~Similar to OVOCs, the spatial variability of aerosol species were greatly reduced ~~inorganic (i.e., ammonium, sulfate, nitrate, chloride) and organic components (i.e., HOA, COA, and OOA) are similar across the ci~~with CV values of~~ty (CV < 0.~~35% vs. 38-84%~~)~~ for the non-haze days.~~, although a few h~~Hot spots of HOA and COA became more evident,~~exist~~ which is consistent with the less-dispersed primary emissions under stagnant conditions (Figure 4)~~ (Figure 1f). The sampling inlets of the PKU mobile lab are located at 3.4 m above the ground, which may sample air from both of urban background and instantaneous plumes. The 40-s $PM_{2.5}$ measurements by TOF-ACSM may roughly represent a maximum area of 0.16 km^2 upwind when the mobile laboratory was run on the 4th Ring Road by cycles.~~ The OOA mass increased most and showed a spatial pattern that were consistent with inorganic species. Unlike the non-haze days, the spatial pattern of ammonium was similar to those of sulfate and nitrate. The ~~similar~~ chemical composition of $PM_{2.5}$ ~~along the road suggests~~became relatively homogeneous ~~spatial distributions of the mass concentration and composition of NR-$PM_{2.5}$ across the city under haze conditions~~during the haze day. The molar ratio of $n_{NH_4^+}$: $(2\times n_{SO_4^{2-}} + n_{NO_3^-})$ was ~1 (Figure 5), suggesting an uniform neutralization pattern over the city during the haze day. ~~This is supported by the fact that the particle composition observed at the PKU roof site was similar to our mobile measurements (Figure S3).~~ Although stagnant conditions facilitate the accumulation of localized ~~-~~emissions, polluted air mass leads to elevated urban background for both primary and secondary pollutants. Previous studies suggest that over 60% of the $PM_{2.5}$ mass in Beijing can be contributed by regional transport during the winter haze event (Sun et al., 2014; Wu et al., 2021). ~~s (e.g., vehicle emissions on the road), over 60% of the $PM_{2.5}$ mass in Beijing can be contributed by regional transport~~

~~during the winter haze episodes . The~~ Secondary formation can also be enhanced because of the elevated precursor concentrations during the haze day and heterogeneous and aqueous pathways that occur during the high RH stage. Our results indicate~~predominant contribution of regional transport suggests similar sources of $PM_{2.5}$ in Beijing. Similar particle composition suggests a~~ a spatial chemical homogeneity perhaps in a regional scale ~~at least on the megacity scale~~ in terms of ~~gas to particle equilibrium or partitioning as well as the heterogeneous or particle phase production~~particle formation ~~. The north-south difference in mass concentration is perhaps driven by the differences in atmospheric dilution on the intracity scale~~ (Sun et al., 2016; Chen et al., 2020). The uniform spatial distributions of PM composition under haze conditions are similar to the observations in the metropolitan area of Zurich when thermal inversions occur over the Swiss plateau and secondary pollution was~~n is~~ built up regionally (Mohr et al., 2011), highlighting stagnant metrological conditions as one of the key drivers of the ~~city-scale~~ chemical homogeneity.

3.3 C~~C~~hemical homogeneity of OVOC formation under haze conditions

Figure 7~~5~~ shows the spatial-temporal variations of the concentrations of the detected VOCs and OVOCs measured during the non-haze and haze ~~periods of the mobile campaign~~days. The concentrations of ∑ hydrocarbons (i.e., aromatics and alkenes) ~~are~~ were the highest in the morning (9:00 a.m. to 11:00 a.m.) for both non-haze and haze periods, which may be explained by shallow boundary layer, rush-hour traffic emissions, and slow chemical removal (de Gouw et al., 2009). The on-road measurements of hydrocarbons ~~are~~ were largely affected by instantaneous vehicle plumes. The greater concentrations of hydrocarbon in the afternoon (2:00 p.m. to 4:00 p.m.) than in the earlier period (11:00 a.m. to 2:00 p.m.) suggest that the mobile measurements captured less vehicle plumes, which is consistent with the less traffic volume on the road. Under non-haze conditions, the spatial variabilit~~ies~~y of hydrocarbons vari~~ed~~ed significantly during the day. Their CV values ~~are~~ were high in the morning and low in the afternoon. It is likely that photochemistry and better mixing conditions in the afternoon smoothed out some of the spatial variability ~~ies~~ caused by the on-road vehicle emissions (Mellouki et al., 2015; Karl et al., 2018). By contrast, their concentrations ~~keep~~ continued ~~decreasing~~ to decrease during the day under haze conditions, and the greater concentrations of ∑ hydrocarbons than during the ~~clean~~ non-haze days ~~are~~ were plausibly driven by the ~~greater contribution of regional transport to on-road air~~polluted urban background levels and ~~stagnant meteorological conditions that favour the accumulation of on-road~~less-dispersed vehicle plumes under stagnant conditions. Under haze conditions, the spatial variability of hydrocarbons ~~is~~ was slightly greater in the afternoon, which ~~is~~ was probably because of the change of regional transport direction. As shown in Figure~~.~~ ~~S4~~S7, the backward trajectories suggest that the air masses gradually shifted from eastern to southern during the haze day. For the two categories of OVOCs, the non-haze temporal variations w~~are~~ere similar to that of hydrocarbons. Their CV values indicate much smaller spatial ~~variabilities~~ variability of OVOCs in the morning rush hour (9:00 a.m. to 11:00 a.m.) than that of hydrocarbons, which~~. This~~ is consistent with previous ~~results of source apportionment~~finding of ~~that~~ the predominant contribution of secondary production ~~is to the main contributor of~~ most OVOCs in Beijing (L. W.

Wang et al., 2021). As the photochemical production proceeds during the day, the spatial variabilitiesy of OVOCs increased and then decreased, similar to that of hydrocarbons. On the other hand, the haze-day temporal and spatial variations of OVOCs are were all similar to that of hydrocarbons (CV < 0.36), corresponding to the predominant contribution of regional transport to the on-road concentrations of these pollutants.

~~3.3 Chemical homogeneity under haze conditions~~

Figure 86 shows the correlation heatmaps of the concentrations of VOCs and OVOCs measured during the clean day and haze day ~~for all measurement cycles~~from 9 a.m. to 4 p.m. on the 4th Ring Road ~~of Beijing~~. ~~Day-to-day variations~~Only two days ~~are~~ were c~~not included~~onsidered in this analysis to avoid inconsistent ~~because of the possible change of~~ source profiles~~s~~. ~~Only~~ pPrimary hydrocarbons showed good correlations with each other during the clean day (Figure ~~6~~8a), which~~. This is~~ was consistent with ~~the~~ predominant contribution of traffic emissions to their on-road concentrations. Secondary species like OVOCs and $PM_{2.5}$ ~~are~~ were more regional and di~~d~~ not correlate with ~~these~~ primary hydrocarbons (Figure ~~S9~~ S13 in the Supplement). They di~~d~~ not correlate with each other either, indicating a spatial chemical heterogeneity in OVOC and $PM_{2.5}$ formation. By contrast, the haze-day heatmaps show significantly different patterns (Figure 86b ~~and Figure S10~~). Primary hydrocarbons correlated well with each other (Pearson~~'s~~ $r > 0.7$, $\alpha = 0.01$). They also showed good positive correlations with many less-oxygenated OVOCs (e.g., aldehydes and ketones with 1-2 oxygen atoms in their formulae (Table ~~S1~~S2). These OVOCs may be contributed by both primary and secondary sources, and they can be formed and accumulated ~~during~~ along the ~~regional~~ transport ~~process~~routes. The NR-$PM_{2.5}$ components also correlated with these VOCs and OVOCs (Figure ~~S9~~S13). Such good spatial-temporal correlations are consistent with the predominant contribution of regional transport to high concentrations of hydrocarbons, less-oxygenated OVOCs, and $PM_{2.5}$ in Beijing during the haze event. Interestingly, more oxygenated OVOCs (e.g., anhydrides and acids with 2-4 oxygen atoms in their formulae) that ~~are~~ were mainly contributed by secondary sources showed good positive correlations with each other ($r > 0.7$, $\alpha = 0.01$) but moderately negative correlations with hydrocarbons and less-oxygenated OVOCs as well as the NR-$PM_{2.5}$ components. These species include CH_2O_2 (tentatively assigned as formic acid), $C_2H_4O_3$, $C_3H_4O_3$, $C_4H_4O_4$, $C_4H_4O_3$, $C_5H_4O_3$, and $C_5H_4O_2$. The spatial-temporal correlations for these more oxygenated OVOCs suggest similar more-oxygenated OVOC composition on the megacity scale during the haze day, which may indicate a homogeneous photochemical production as well as gas-to-particle partitioning. Figure 14 in the Supplement shows similar correlations that were observed in another haze event in January 2021.

High oxidation capacity in winter in NCP has been reported (Lu et al., 2019a; Slater et al., 2020). Secondary OVOCs ~~are~~ can be formed and accumulated along the transport routes. With a rather uniform distribution of hydroxyl radical which likely happens under winter haze conditions because of the thick cloud cover and increased particle scattering, the formation of more-oxygenated OVOCs from less-oxygenated OVOCs can be relatively homogeneous in the city. Although these more-oxygenated OVOCs may partition to the particle phase, the gas-to-particle partitioning ~~are~~ were not expected to affect much the spatial variability of the more-oxygenated OVOCs because of the similar chemical composition of $PM_{2.5}$ and the narrow loading range on the intracity scale under haze conditions. The secondary production can thus explain~~s~~ the negative correlations

of the more-oxygenated OVOCs with their precursors (e.g., hydrocarbon and less-oxygenated OVOCs) and $PM_{2.5}$. Moreover, the gas-particle repartitioning caused by temperature difference may affect the distribution of more-oxygenated OVOCs. This effect is however expected to be minor considering the range of OA loadings, the vapor pressures of these more-oxygenated OVOCs, and the possible temperature elevation of 1-3 °C in the city (Chen et al., 2020; Wang et al., 2020; Yang et al., 2013). Peroxyacetyl nitrate (PAN, $C_2H_4O_3$) is more sensitive to temperature and less stable than the other more-oxygenated OVOCs (Seinfeld and Pandis, 2016), which may explain its lower correlation coefficient in Fig. 6bure 8b.

4 Conclusions

In this study, we conducted on-road mobile measurements of air pollutants including NR-$PM_{2.5}$ and its components, gaseous pollutants, VOCs, and OVOCs under different pollution levels in winter in Beijing. During the clean periodsnon-haze days, large spatial variabilities of these pollutants are were observed, which can be largely attributed to the influence of localized sources, chemical reaction, and secondary productionmeteorological conditions. In particular, the inorganic composition of NR-$PM_{2.5}$ varied greatly, indicating a wide range of particle neutralization on the intracity scale under less polluted conditions in winter Beijing. For OA, tThe spatial variabilities are driven byof local HOA and COA were driven by vehicle and cooking emissions as well as atmospheric dilutionOOA. The spatial variations of regular gas pollutants are relatively smaller than those of the $PM_{2.5}$ components. The spatial distributions of the concentrations of patterns of VOCs and OVOCs varied by species. Detected Hhydrocarbons (i.e. mostly aromatic species) are were largely greatly affected by on road vehicle emissions and showed greater PF values than OVOCs did, and thus show large spatial variabilities during the clean periods. Our results suggest about 30–40% contributions of high-emitting plumes to the on-road concentrations of aromatic species during the clean periods compared with 9–13% during the haze periods. Secondary OVOCs showed the greatest spatial variability, indicating a large heterogeneity in their formation during the non-haze days. Overall, tThe great spatial heterogeneity of the particle composition and VOCs may challenge the development of future pollution control strategies as clean air actions continue. The results also indicate different and accurate evaluation of human exposures to particles and gaseous pollutants on the intracity scale, which requires fine-resolution models to evaluate in the megacity. On the other hand,

During the haze days, stagnant weather conditions the spatial variability of secondary gaseous and aerosol pollutants and predominant contributions were largely reduced during the haze dayfrom regional transport to urban background concentrations of particulate and gaseous pollutants largely reduce the spatial variabilities of these pollutants in the megacity. More-oxygenated OVOCs showed good positive correlation among themselves but moderate negative correlations with hydrocarbons, less-oxygenated OVOCs, and $PM_{2.5}$ componentsaerosol species, suggesting a spatially homogeneous photochemical chemical production as well as gas-to-particle partitioning on the megacity scale. Such a chemical homogeneity of OVOC formation may lead to efficient local production of semivolatile oxidation products that enhances the SOA production in the megacity to enhance theand the haze development.

Data availability. Data presented in this manuscript are available upon request to the corresponding author.

Author contributions. KL conducted the measurements and data analysis with the help of QC, RK, YL, YZ, XC, TJ, XL, SC, and GH. QC, RK, and KL wrote the manuscript.

Competing interests. The authors declare no competing financial interests.

Acknowledgements. This work was supported by the National Natural Science Foundation of China (91544107, 41875165, and 41961134034~~, and 51861135102~~) and the 111 Project of Urban Air Pollution and Health Effects (B20009). The authors thank Theodore K. Koenig for helpful discussions.

References

Apte, J. S., Messier, K. P., Gani, S., Brauer, M., Kirchstetter, T. W., Lunden, M. M., Marshall, J. D., Portier, C. J., Vermeulen, R. C. H., and Hamburg, S. P.: High-resolution air pollution mapping with Google street view cars: Exploiting big data, Environ. Sci. Technol., 51, 6999-7008, https://doi.org/10.1021/acs.est.7b00891, 2017.

Bell, M. L., Peng, R. D., and Dominici, F.: The exposure-response curve for ozone and risk of mortality and the adequacy of current ozone regulations, Environ. Health Perspect., 114, 532-536, https://doi.org/10.1289/ehp.8816, 2006.

Canagaratna, M. R., Jayne, J. T., Jimenez, J. L., Allan, J. D., Alfarra, M. R., Zhang, Q., Onasch, T. B., Drewnick, F., Coe, H., Middlebrook, A., Delia, A., Williams, L. R., Trimborn, A. M., Northway, M. J., DeCarlo, P. F., Kolb, C. E., Davidovits, P., and Worsnop, D. R.: Chemical and microphysical characterization of ambient aerosols with the aerodyne aerosol mass spectrometer, Mass Spectrom. Rev., 26, 185-222, https://doi.org/10.1002/mas.20115, 2007.

Chang, X., Wang, S. X., Zhao, B., Xing, J., Liu, X. X., Wei, L., Song, Y., Wu, W. J., Cai, S. Y., Zheng, H. T., Ding, D., and Zheng, M.: Contributions of inter-city and regional transport to PM2.5 concentrations in the Beijing-Tianjin-Hebei region and its implications on regional joint air pollution control, Sci. Total Environ., 660, 1191-1200, https://doi.org/10.1016/j.scitotenv.2018.12.474, 2019.

Chen, J. H., Wang, W., Liu, H. J., and Ren, L. H.: Determination of road dust loadings and chemical characteristics using resuspension, Environ. Monit. Assess., 184, 1693-1709, https://doi.org/10.1007/s10661-011-2071-1, 2012.

Chen, Y., Cai, J., Wang, Z. C., Peng, C., Yao, X. J., Tian, M., Han, Y. Q., Shi, G. M., Shi, Z. B., Liu, Y., Yang, X., Zheng, M., Zhu, T., He, K. B., Zhang, Q., and Yang, F. M.: Simultaneous measurements of urban and rural particles in Beijing - Part 1: Chemical composition and mixing state, Atmos. Chem. Phys., 20, 9231-9247, https://doi.org/10.5194/acp-20-9231-2020, 2020.

Cheng, X., Chen, Q., Li, Y., Huang, G., Liu, Y., Lu, S., Zheng, Y., Qiu, W., Lu, K., Qiu, X., Bianchi, F., Yan, C., Yuan, B., Shao, M., Wang, Z., Canagaratna, M. R., Zhu, T., Wu, Y., and Zeng, L.: Secondary production of gaseous nitrated phenols in polluted urban environments, Environ. Sci. Technol., https://doi.org/10.1021/acs.est.0c07988, 2021.

de Gouw, J. A., Middlebrook, A. M., Warneke, C., Goldan, P. D., Kuster, W. C., Roberts, J. M., Fehsenfeld, F. C., Worsnop, D. R., Canagaratna, M. R., Pszenny, A. A. P., Keene, W. C., Marchewka, M., Bertman, S. B., and Bates, T. S.: Budget of organic carbon in a polluted atmosphere: Results from the New England Air Quality Study in 2002, J. Geophys. Res-Atmos., 110, 22, https://doi.org/10.1029/2004jd005623, 2005.

de Gouw, J. A., Welsh-Bon, D., Warneke, C., Kuster, W. C., Alexander, L., Baker, A. K., Beyersdorf, A. J., Blake, D. R., Canagaratna, M., Celada, A. T., Huey, L. G., Junkermann, W., Onasch, T. B., Salcido, A., Sjostedt, S. J., Sullivan, A. P., Tanner, D. J., Vargas, O., Weber, R. J., Worsnop, D. R., Yu, X. Y., and Zaveri, R.: Emission and chemistry of organic carbon in the gas and aerosol phase at a sub-urban site near Mexico City in March 2006 during the MILAGRO study, Atmos. Chem. Phys., 9, 3425-3442, https://doi.org/10.5194/acp-9-3425-2009, 2009.

Deng, F. Y., Lv, Z. F., Qi, L. J., Wang, X. T., Shi, M. S., and Liu, H.: A big data approach to improving the vehicle emission inventory in China, Nat. Commun., 11, 12, https://doi.org/10.1038/s41467-020-16579-w, 2020.

Duan, J., Huang, R. J., Li, Y. J., Chen, Q., Zheng, Y., Chen, Y., Lin, C. S., Ni, H. Y., Wang, M., Ovadnevaite, J., Ceburnis, D., Chen, C. Y., Worsnop, D. R., Hoffmann, T., O'Dowd, C., and Cao, J. J.: Summertime and wintertime atmospheric processes of secondary aerosol in Beijing, Atmos. Chem. Phys., 20, 3793-3807, https://doi.org/10.5194/acp-20-3793-2020, 2020.

Elser, M., Bozzetti, C., El-Haddad, I., Maasikmets, M., Teinemaa, E., Richter, R., Wolf, R., Slowik, J. G., Baltensperger, U., and Prevot, A. S. H.: Urban increments of gaseous and aerosol pollutants and their sources using mobile aerosol mass spectrometry measurements, Atmos. Chem. Phys., 16, 7117-7134, https://doi.org/10.5194/acp-16-7117-2016, 2016.

Ge, B. Z., Wang, Z. F., Lin, W. L., Xu, X. B., Li, J., Ji, D. S., and Ma, Z. Q.: Air pollution over the North China Plain and its implication of regional transport: A new sight from the observed evidences, Environ. Pollut., 234, 29-38, https://doi.org/10.1016/j.envpol.2017.10.084, 2018.

Gentner, D. R., Jathar, S. H., Gordon, T. D., Bahreini, R., Day, D. A., El Haddad, I., Hayes, P. L., Pieber, S. M., Platt, S. M., de Gouw, J., Goldstein, A. H., Harley, R. A., Jimenez, J. L., Prevot, A. S. H., and Robinson, A. L.: Review of urban secondary organic aerosol formation from gasoline and diesel motor vehicle emissions, Environ. Sci. Technol., 51, 1074-1093, https://doi.org/10.1021/acs.est.6b04509, 2017.

Gu, P. S., Li, H., Ye, Q., Robinson, E. S., Apte, J. S., Robinson, A. L., and Presto, A. A.: Intracity variability of particulate matter exposure is driven by carbonaceous sources and correlated with land-use variables, Environ. Sci. Technol., 52, 11545-11554, https://doi.org/10.1021/acs.est.8b03833, 2018.

Guo, H., Ling, Z. H., Cheng, H. R., Simpson, I. J., Lyu, X. P., Wang, X. M., Shao, M., Lu, H. X., Ayoko, G., Zhang, Y. L., Saunders, S. M., Lam, S. H. M., Wang, J. L., and Blake, D. R.: Tropospheric volatile organic compounds in China, Sci. Total Environ., 574, 1021-1043, https://doi.org/10.1016/j.scitotenv.2016.09.116, 2017.

Huang, G. C., Liu, Y., Shao, M., Li, Y., Chen, Q., Zheng, Y., Wu, Z. J., Liu, Y. C., Wu, Y. S., Hu, M., Li, X., Lu, S. H., Wang, C. J., Liu, J. Y., Zheng, M., and Zhu, T.: Potentially important contribution of gas-phase oxidation of naphthalene and methylnaphthalene to secondary organic aerosol during haze events in Beijing, Environ. Sci. Technol., 53, 1235-1244, https://doi.org/10.1021/acs.est.8b04523, 2019.

Huang, R. J., Zhang, Y. L., Bozzetti, C., Ho, K. F., Cao, J. J., Han, Y. M., Daellenbach, K. R., Slowik, J. G., Platt, S. M., Canonaco, F., Zotter, P., Wolf, R., Pieber, S. M., Bruns, E. A., Crippa, M., Ciarelli, G., Piazzalunga, A., Schwikowski, M., Abbaszade, G., Schnelle-Kreis, J., Zimmermann, R., An, Z. S., Szidat, S., Baltensperger, U., El Haddad, I., and Prevot, A. S. H.: High secondary aerosol contribution to particulate pollution during haze events in China, Nature, 514, 218-222, https://doi.org/10.1038/nature13774, 2014.

Karl, T., Striednig, M., Graus, M., Hammerle, A., and Wohlfahrt, G.: Urban flux measurements reveal a large pool of oxygenated volatile organic compound emissions, Proc. Natl. Acad. Sci. U. S. A., 115, 1186-1191, https://doi.org/10.1073/pnas.1714715115, 2018.

Khuzestani, R. B., Schauer, J. J., Wei, Y. J., Zhang, L. L., Cai, T. Q., Zhang, Y., and Zhang, Y. X.: Quantification of the sources of long-range transport of PM2.5 pollution in the Ordos region, Inner Mongolia, China, Environ. Pollut., 229, 1019-1031, https://doi.org/10.1016/j.envpol.2017.07.093, 2017.

Kolb, C. E., Herndon, S. C., McManus, B., Shorter, J. H., Zahniser, M. S., Nelson, D. D., Jayne, J. T., Canagaratna, M. R., and Worsnop, D. R.: Mobile laboratory with rapid response instruments for real-time measurements of urban and regional trace gas and particulate distributions and emission source characteristics, Environ. Sci. Technol., 38, 5694-5703, https://doi.org/10.1021/es030718p, 2004.

Lei, L., Zhou, W., Chen, C., He, Y., Li, Z. J., Sun, J. X., Tang, X., Fu, P. Q., Wang, Z. F., and Sun, Y. L.: Long-term characterization of aerosol chemistry in cold season from 2013 to 2020 in Beijing, China, Environ. Pollut., 268, 9, https://doi.org/10.1016/j.envpol.2020.115952, 2021.

Li, J., Wu, R. R., Li, Y. Q., Hao, Y. F., Xie, S. D., and Zeng, L. M.: Effects of rigorous emission controls on reducing ambient volatile organic compounds in Beijing, China, Sci. Total Environ., 557, 531-541, https://doi.org/10.1016/j.scitotenv.2016.03.140, 2016.

Li, J., Han, Z. W., Sun, Y. L., Li, J. W., and Liang, L.: Chemical formation pathways of secondary organic aerosols in the Beijing-Tianjin-Hebei region in wintertime, Atmos. Environ., 244, 15, https://doi.org/10.1016/j.atmosenv.2020.117996, 2021.

Li, Y. J., Sun, Y., Zhang, Q., Li, X., Li, M., Zhou, Z., and Chan, C. K.: Real-time chemical characterization of atmospheric particulate matter in China: A review, Atmos. Environ., 158, 270-304, https://doi.org/10.1016/j.atmosenv.2017.02.027, 2017.

Liang, Q., Bao, X., Sun, Q., Zhang, Q., Zou, X., Huang, C., Shen, C., and Chu, Y.: Imaging VOC distribution in cities and tracing VOC emission sources with a novel mobile proton transfer reaction mass spectrometer, Environ. Pollut., 265, https://doi.org/10.1016/j.envpol.2020.114628, 2020.

Liao, K., Chen, Q., Liu, Y., Li, Y. J., Lambe, A. T., Zhu, T., Huang, R.-J., Zheng, Y., Cheng, X., Miao, R., Huang, G., Khuzestani, R. B., and Jia, T.: Secondary organic aerosol formation of fleet vehicle emissions in China: Potential seasonality of spatial distributions, Environ. Sci. Technol., https://doi.org/10.1021/acs.est.0c08591, 2021.

Liu, J., Han, Y. Q., Tang, X., Zhu, J., and Zhu, T.: Estimating adult mortality attributable to PM2.5 exposure in China with assimilated PM2.5 concentrations based on a ground monitoring network, Sci. Total Environ., 568, 1253-1262, https://doi.org/10.1016/j.scitotenv.2016.05.165, 2016.

Liu, Y. F., Song, M. D., Liu, X. G., Zhang, Y. P., Hui, L. R., Kong, L. W., Zhang, Y. Y., Zhang, C., Qu, Y., An, J. L., Ma, D. P., Tan, Q. W., and Feng, M.: Characterization and sources of volatile organic compounds (VOCs) and their related

changes during ozone pollution days in 2016 in Beijing, China, Environ. Pollut., 257, 12, https://doi.org/10.1016/j.envpol.2019.113599, 2020.

Lu, K. D., Fuchs, H., Hofzumahaus, A., Tan, Z. F., Wang, H. C., Zhang, L., Schmitt, S. H., Rohrer, F., Bohn, B., Broch, S., Dong, H. B., Gkatzelis, G. I., Hohaus, T., Holland, F., Li, X., Liu, Y., Liu, Y. H., Ma, X. F., Novelli, A., Schlag, P., Shao, M., Wu, Y. S., Wu, Z. J., Zeng, L. M., Hu, M., Kiendler-Scharr, A., Wahner, A., and Zhang, Y. H.: Fast photochemistry in wintertime haze: Consequences for pollution mitigation strategies, Environ. Sci. Technol., 53, 10676-10684, https://doi.org/10.1021/acs.est.9b02422, 2019a.

Lu, K. D., Guo, S., Tan, Z. F., Wang, H. C., Shang, D. J., Liu, Y. H., Li, X., Wu, Z. J., Hu, M., and Zhang, Y. H.: Exploring atmospheric free-radical chemistry in China: the self-cleansing capacity and the formation of secondary air pollution, Natl. Sci. Rev., 6, 579-594, https://doi.org/10.1093/nsr/nwy073, 2019b.

Lv, Z. F., Wang, X. T., Deng, F. Y., Ying, Q., Archibald, A. T., Jones, R. L., Ding, Y., Cheng, Y., Fu, M. L., Liu, Y., Man, H. Y., Xue, Z. G., He, K. B., Hao, J. M., and Liu, H. A.: Source-Receptor Relationship Revealed by the Halted Traffic and Aggravated Haze in Beijing during the COVID-19 Lockdown, Environ. Sci. Technol., 54, 15660-15670, https://doi.org/10.1021/acs.est.0c04941, 2020.

Mellouki, A., Wallington, T. J., and Chen, J.: Atmospheric chemistry of oxygenated volatile organic compounds: Impacts on air quality and climate, Chem. Rev., 115, 3984-4014, https://doi.org/10.1021/cr500549n, 2015.

Miao, R., Chen, Q., Shrivastava, M., Chen, Y., Zhang, L., Hu, J., Zheng, Y., and Liao, K.: Process-based and observation-constrained SOA simulations in China: the role of semivolatile and intermediate-volatility organic compounds and OH levels, Atmos. Chem. Phys., 21, 16183-16201, https://doi.org/10.5194/acp-21-16183-2021, 2021.

Mo, Z. W., Shao, M., and Lu, S. H.: Compilation of a source profile database for hydrocarbon and OVOC emissions in China, Atmos. Environ., 143, 209-217, https://doi.org/10.1016/j.atmosenv.2016.08.025, 2016.

Mo, Z. W., Huang, S., Yuan, B., Pei, C. L., Song, Q. C., Qi, J. P., Wang, M., Wang, B. L., Wang, C., Li, M., Zhang, Q., and Shao, M.: Deriving emission fluxes of volatile organic compounds from tower observation in the Pearl River Delta, China, Sci. Total Environ., 741, 9, https://doi.org/10.1016/j.scitotenv.2020.139763, 2020.

Mohr, C., Richter, R., DeCarlo, P. F., Prevot, A. S. H., and Baltensperger, U.: Spatial variation of chemical composition and sources of submicron aerosol in Zurich during wintertime using mobile aerosol mass spectrometer data, Atmos. Chem. Phys., 11, 7465-7482, https://doi.org/10.5194/acp-11-7465-2011, 2011.

Mozaffar, A., and Zhang, Y. L.: Atmospheric Volatile Organic Compounds (VOCs) in China: a Review, Curr. Pollut. Rep., 6, 250-263, https://doi.org/10.1007/s40726-020-00149-1, 2020.

Nenes, A., Pandis, S. N., Weber, R. J., and Russell, A.: Aerosol pH and liquid water content determine when particulate matter is sensitive to ammonia and nitrate availability, Atmos. Chem. Phys., 20, 3249-3258, https://doi.org/10.5194/acp-20-3249-2020, 2020.

Pan, Y. P., Tian, S. L., Liu, D. W., Fang, Y. T., Zhu, X. Y., Gao, M., Wentworth, G. R., Michalski, G., Huang, X. J., and Wang, Y. S.: Source apportionment of aerosol ammonium in an ammonia-rich atmosphere: An isotopic study of summer clean and hazy days in urban Beijing, J. Geophys. Res-Atmos., 123, 5681-5689, https://doi.org/10.1029/2017jd028095, 2018.

Peng, J. F., Hu, M., Shang, D. J., Wu, Z. J., Du, Z. F., Tan, T. Y., Wang, Y. N., Zhang, F., and Zhang, R. Y.: Explosive Secondary Aerosol Formation during Severe Haze in the North China Plain, Environ. Sci. Technol., 55, 2189-2207, https://doi.org/10.1021/acs.est.0c07204, 2021.

Qi, J., Zheng, B., Li, M., Yu, F., Chen, C. C., Liu, F., Zhou, X. F., Yuan, J., Zhang, Q., and He, K. B.: A high-resolution air pollutants emission inventory in 2013 for the Beijing-Tianjin-Hebei region, China, Atmos. Environ., 170, 156-168, https://doi.org/10.1016/j.atmosenv.2017.09.039, 2017.

Quan, J. N., and Jia, X. C.: Review of aircraft measurements over China: aerosol, atmospheric photochemistry, and cloud, Atmos. Res., 243, 14, https://doi.org/10.1016/j.atmosres.2020.104972, 2020.

Seinfeld, J. H., and Pandis, S. N.: Atmospheric Chemistry and Physics: From Air Pollution to Climate Change, Third Edition ed., John Wiley & Sons, Inc., Hoboken, New Jersey, 2016.

Slater, E. J., Whalley, L. K., Woodward-Massey, R., Ye, C. X., Lee, J. D., Squires, F., Hopkins, J. R., Dunmore, R. E., Shaw, M., Hamilton, J. F., Lewis, A. C., Crilley, L. R., Kramer, L., Bloss, W., Vu, T., Sun, Y. L., Xu, W. Q., Yue, S. Y., Ren, L. J., Acton, W. J. F., Hewitt, C. N., Wang, X. M., Fu, P. Q., and Heard, D. E.: Elevated levels of OH observed in haze events during wintertime in central Beijing, Atmos. Chem. Phys., 20, 14847-14871, https://doi.org/10.5194/acp-20-14847-2020, 2020.

Song, M. D., Li, X., Yang, S. D., Yu, X. N., Zhou, S. X., Yang, Y. M., Chen, S. Y., Dong, H. B., Liao, K. R., Chen, Q., Lu, K. D., Zhang, N. N., Cao, J. J., Zeng, L. M., and Zhang, Y. H.: Spatiotemporal variation, sources, and secondary transformation potential of volatile organic compounds in Xi'an, China, Atmos. Chem. Phys., 21, 4939-4958, https://doi.org/10.5194/acp-21-4939-2021, 2021.

Stein, A. F., Draxler, R. R., Rolph, G. D., Stunder, B. J. B., Cohen, M. D., and Ngan, F.: NOAA'S hysplit atmospheric transport and dispersion modeling system, Bull. Amer. Meteorol. Soc., 96, 2059-2077, https://doi.org/10.1175/bams-d-14-00110.1, 2015.

Sun, J., Wang, Y. S., Wu, F. K., Tang, G. Q., Wang, L. L., Wang, Y. H., and Yang, Y.: Vertical characteristics of VOCs in the lower troposphere over the North China Plain during pollution periods, Environ. Pollut., 236, 907-915, https://doi.org/10.1016/j.envpol.2017.10.051, 2018.

Sun, K., Tao, L., Miller, D. J., Pan, D., Golston, L. M., Zondlo, M. A., Griffin, R. J., Wallace, H. W., Leong, Y. J., Yang, M. M., Zhang, Y., Mauzerall, D. L., and Zhu, T.: Vehicle emissions as an important urban ammonia source in the United States and China, Environ. Sci. Technol., 51, 2472-2481, https://doi.org/10.1021/acs.est.6b02805, 2017.

Sun, Y. L., Jiang, Q., Wang, Z. F., Fu, P. Q., Li, J., Yang, T., and Yin, Y.: Investigation of the sources and evolution processes of severe haze pollution in Beijing in January 2013, J. Geophys. Res-Atmos., 119, 4380-4398, https://doi.org/10.1002/2014jd021641, 2014.

Sun, Y. L., Wang, Z. F., Du, W., Zhang, Q., Wang, Q. Q., Fu, P. Q., Pan, X. L., Li, J., Jayne, J., and Worsnop, D. R.: Long-term real-time measurements of aerosol particle composition in Beijing, China: seasonal variations, meteorological effects, and source analysis, Atmos. Chem. Phys., 15, 10149-10165, https://doi.org/10.5194/acp-15-10149-2015, 2015.

Sun, Y. L., Chen, C., Zhang, Y. J., Xu, W. Q., Zhou, L. B., Cheng, X. L., Zheng, H. T., Ji, D. S., Li, J., Tang, X., Fu, P. Q., and Wang, Z. F.: Rapid formation and evolution of an extreme haze episode in Northern China during winter 2015, Sci. Rep., 6, 9, https://doi.org/10.1038/srep27151, 2016.

Sun, Y. L., He, Y., Kuang, Y., Xu, W. Y., Song, S. J., Ma, N., Tao, J. C., Cheng, P., Wu, C., Su, H., Cheng, Y. F., Xie, C. H., Chen, C., Lei, L., Qiu, Y. M., Fu, P. Q., Croteau, P., and Worsnop, D. R.: Chemical Differences Between PM1 and PM2.5 in Highly Polluted Environment and Implications in Air Pollution Studies, Geophys. Res. Lett., 47, 10, https://doi.org/10.1029/2019gl086288, 2020.

Tan, Y., Lipsky, E. M., Saleh, R., Robinson, A. L., and Presto, A. A.: Characterizing the spatial variation of air pollutants and the contributions of high emitting vehicles in Pittsburgh, PA, Environ. Sci. Technol., 48, 14186-14194, https://doi.org/10.1021/es5034074, 2014.

Wang, L. W., Slowik, J. G., Tong, Y. D., Duan, J., Gu, Y. F., Rai, P., Qi, L., Stefenelli, G., Baltensperger, U., Huang, R. J., Cao, J. J., and Prevot, A. S. H.: Characteristics of wintertime VOCs in urban Beijing: Composition and source apportionment, Atmos. Environ-X, 9, 12, https://doi.org/10.1016/j.aeaoa.2020.100100, 2021.

Wang, M., Zhu, T., Zheng, J., Zhang, R. Y., Zhang, S. Q., Xie, X. X., Han, Y. Q., and Li, Y.: Use of a mobile laboratory to evaluate changes in on-road air pollutants during the Beijing 2008 Summer Olympics, Atmos. Chem. Phys., 9, 8247-8263, https://doi.org/10.5194/acp-9-8247-2009, 2009.

Wang, M., Zhu, T., Zhang, J. P., Zhang, Q. H., Lin, W. W., Li, Y., and Wang, Z. F.: Using a mobile laboratory to characterize the distribution and transport of sulfur dioxide in and around Beijing, Atmos. Chem. Phys., 11, 11631-11645, https://doi.org/10.5194/acp-11-11631-2011, 2011.

Wang, Q., Zhang, C., Ren, C., Hang, J., and Li, Y. G.: Urban heat island circulations over the Beijing-Tianjin region under calm and fair conditions, Build. Environ., 180, 12, https://doi.org/10.1016/j.buildenv.2020.107063, 2020.

Wang, T., Xue, L. K., Brimblecombe, P., Lam, Y. F., Li, L., and Zhang, L.: Ozone pollution in China: A review of concentrations, meteorological influences, chemical precursors, and effects, Sci. Total Environ., 575, 1582-1596, https://doi.org/10.1016/j.scitotenv.2016.10.081, 2017.

Wang, W. G., Liu, M. Y., Wang, T. T., Song, Y., Zhou, L., Cao, J. J., Hu, J. N., Tang, G. G., Chen, Z., Li, Z. J., Xu, Z. Y., Peng, C., Lian, C. F., Chen, Y., Pan, Y. P., Zhang, Y. H., Sun, Y. L., Li, W. J., Zhu, T., Tian, H. Z., and Ge, M. F.: Sulfate formation is dominated by manganese-catalyzed oxidation of SO2 on aerosol surfaces during haze events, Nat. Commun., 12, 10, https://doi.org/10.1038/s41467-021-22091-6, 2021.

Wang, X., Cai, Y. J., Wang, J. J., and Zhao, Y. F.: Concentration monitoring of volatile organic compounds and ozone in Xi'an based on PTR-TOF-MS and differential absorption lidar, Atmos. Environ., 245, 12, https://doi.org/10.1016/j.atmosenv.2020.118045, 2021.

Wang, Y. H., Hu, B., Ji, D. S., Liu, Z. R., Tang, G. Q., Xin, J. Y., Zhang, H. X., Song, T., Wang, L. L., Gao, W. K., Wang, X. K., and Wang, Y. S.: Ozone weekend effects in the Beijing-Tianjin-Hebei metropolitan area, China, Atmos. Chem. Phys., 14, 2419-2429, https://doi.org/10.5194/acp-14-2419-2014, 2014.

Wu, F. C., Xie, P. H., Li, A., Mou, F. S., Chen, H., Zhu, Y., Zhu, T., Liu, J. G., and Liu, W. Q.: Investigations of temporal and spatial distribution of precursors SO2 and NO2 vertical columns in the North China Plain using mobile DOAS, Atmos. Chem. Phys., 18, 1535-1554, https://doi.org/10.5194/acp-18-1535-2018, 2018.

Wu, J. R., Bei, N. F., Wang, Y., Li, X., Liu, S. X., Liu, L., Wang, R. N., Yu, J. Y., Le, T. H., Zuo, M., Shen, Z. X., Cao, J. J., Tie, X. X., and Li, G. H.: Insights into particulate matter pollution in the North China Plain during wintertime: local contribution or regional transport?, Atmos. Chem. Phys., 21, 2229-2249, https://doi.org/10.5194/acp-21-2229-2021, 2021.

Wu, Y., Zhang, S. J., Hao, J. M., Liu, H., Wu, X. M., Hu, J. N., Walsh, M. P., Wallington, T. J., Zhang, K. M., and Stevanovic, S.: On-road vehicle emissions and their control in China: A review and outlook, Sci. Total Environ., 574, 332-349, https://doi.org/10.1016/j.scitotenv.2016.09.040, 2017.

Yang, B., Zhang, K. M., Xu, W. D., Zhang, S. J., Batterman, S., Baldauf, R. W., Deshmukh, P., Snow, R., Wu, Y., Zhang, Q., Li, Z. H., and Wu, X.: On-road chemical transformation as an important mechanism of NO2 formation, Environ. Sci. Technol., 52, 4574-4582, https://doi.org/10.1021/acs.est.7b05648, 2018.

Yang, P., Ren, G. Y., and Liu, W. D.: Spatial and temporal characteristics of Beijing urban heat island intensity, J. Appl. Meteorol. Climatol., 52, 1803-1816, https://doi.org/10.1175/jamc-d-12-0125.1, 2013.

Yang, W. Y., Li, J., Wang, W. G., Li, J. L., Ge, M. F., Sun, Y. L., Chen, X. S., Ge, B. Z., Tong, S. R., Wang, Q. Q., and Wang, Z. F.: Investigating secondary organic aerosol formation pathways in China during 2014, Atmos. Environ., 213, 133-147, https://doi.org/10.1016/j.atmosenv.2019.05.057, 2019.

Ye, Q., Gu, P., Li, H. Z., Robinson, E. S., Lipsky, E., Kaltsonoudis, C., Lee, A. K. Y., Apte, J. S., Robinson, A. L., Sullivan, R. C., Presto, A. A., and Donahue, N. M.: Spatial variability of sources and mixing state of atmospheric particles in a metropolitan area, Environ. Sci. Technol., 52, 6807-6815, https://doi.org/10.1021/acs.est.8b01011, 2018.

Yuan, B., Koss, A. R., Warneke, C., Coggon, M., Sekimoto, K., and de Gouw, J. A.: Proton-transfer-reaction mass spectrometry: Applications in atmospheric sciences, Chem. Rev., 117, 13187-13229, https://doi.org/10.1021/acs.chemrev.7b00325, 2017.

Zhang, Q., Zheng, Y. X., Tong, D., Shao, M., Wang, S. X., Zhang, Y. H., Xu, X. D., Wang, J. N., He, H., Liu, W. Q., Ding, Y. H., Lei, Y., Li, J. H., Wang, Z. F., Zhang, X. Y., Wang, Y. S., Cheng, J., Liu, Y., Shi, Q. R., Yan, L., Geng, G. N., Hong, C. P., Li, M., Liu, F., Zheng, B., Cao, J. J., Ding, A. J., Gao, J., Fu, Q. Y., Huo, J. T., Liu, B. X., Liu, Z. R., Yang, F. M., He, K. B., and Hao, J. M.: Drivers of improved PM2.5 air quality in China from 2013 to 2017, Proc. Natl. Acad. Sci. U. S. A., 116, 24463-24469, https://doi.org/10.1073/pnas.1907956116, 2019.

Zheng, B., Tong, D., Li, M., Liu, F., Hong, C. P., Geng, G. N., Li, H. Y., Li, X., Peng, L. Q., Qi, J., Yan, L., Zhang, Y. X., Zhao, H. Y., Zheng, Y. X., He, K. B., and Zhang, Q.: Trends in China's anthropogenic emissions since 2010 as the consequence of clean air actions, Atmos. Chem. Phys., 18, 14095-14111, https://doi.org/10.5194/acp-18-14095-2018, 2018.

Zheng, Y., Cheng, X., Liao, K. R., Li, Y. W., Li, Y. J., Hu, W. W., Liu, Y., Zhu, T., Chen, S. Y., Zeng, L. M., Worsnop, D., Chen, Q., and Huang, R. J.: Characterization of anthropogenic organic aerosols by TOF-ACSM with the new capture vaporizer, Atmos. Meas. Tech., 13, 2457-2472, https://doi.org/10.5194/amt-13-2457-2020, 2020.

Zheng, Y., Chen, Q., Cheng, X., Mohr, C., Cai, J., Huang, W., Shrivastava, M., Ye, P., Fu, P., Shi, X., Ge, Y., Liao, K., Miao, R., Qiu, X., Koenig, T. K., and Chen, S.: Precursors and Pathways Leading to Enhanced Secondary Organic Aerosol Formation during Severe Haze Episodes, Environ. Sci. Technol., 55, 15680-15693, https://doi.org/10.1021/acs.est.1c04255, 2021.

Zhou, W., Sun, Y. L., Xu, W. Q., Zhao, X. J., Wang, Q. Q., Tang, G. Q., Zhou, L. B., Chen, C., Du, W., Zhao, J., Xie, C. H., Fu, P. Q., and Wang, Z. F.: Vertical characterization of aerosol particle composition in Beijing, China: Insights from 3-month measurements with two aerosol mass spectrometers, J. Geophys. Res-Atmos., 123, 13016-13029, https://doi.org/10.1029/2018jd029337, 2018.

Zhu, Y., Zhang, J. P., Wang, J. X., Chen, W. Y., Han, Y. Q., Ye, C. X., Li, Y. R., Liu, J., Zeng, L. M., Wu, Y. S., Wang, X. F., Wang, W. X., Chen, J. M., and Zhu, T.: Distribution and sources of air pollutants in the North China Plain based on on-road mobile measurements, Atmos. Chem. Phys., 16, 12551-12565, https://doi.org/10.5194/acp-16-12551-2016, 2016.

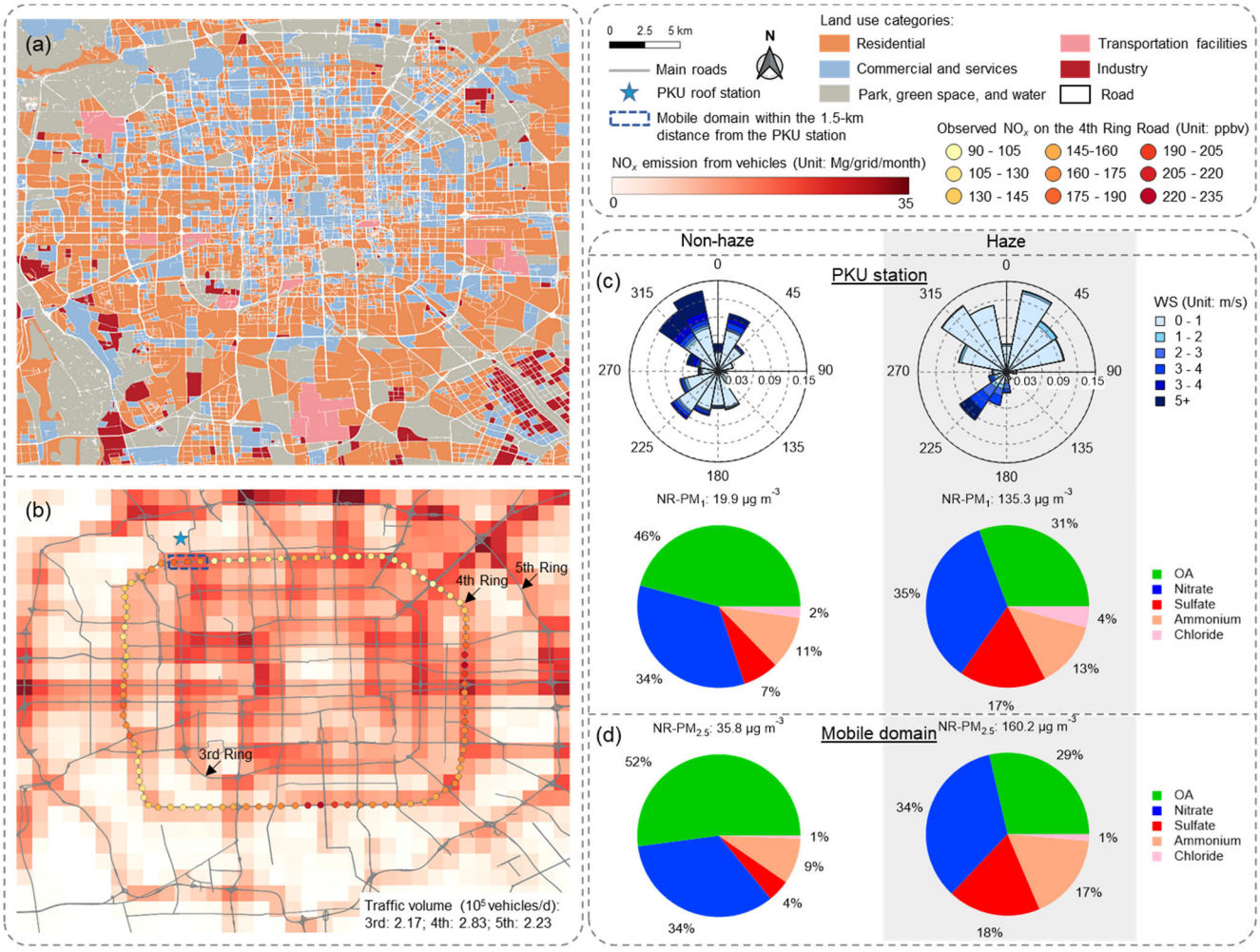

Figure 1. (a) Land use categories in the area of Beijing that were taken from the Mapping Essential Urban Land Use Categories in China (EULUC-China) database (Gong et al., 2020). (b) Monthly NO_x emissions from vehicle provided by Yang et al. (2019) in November 2018 and the mean NO_x concentrations observed by the mobile laboratory between 9 a.m. to 4 p.m. during the non-haze measurement period on the 4th Ring Road in Beijing. (c) Wind rose diagrams and the average non-refractory chemical composition of aerosol particles measured by the LTOF-AMS at the PKU roof site and by the TOF-ACSM on the mobile lab on the 4th Ring Road within the distance of 1.5 km from the roof site. Base maps are provided by OpenStreetMap.

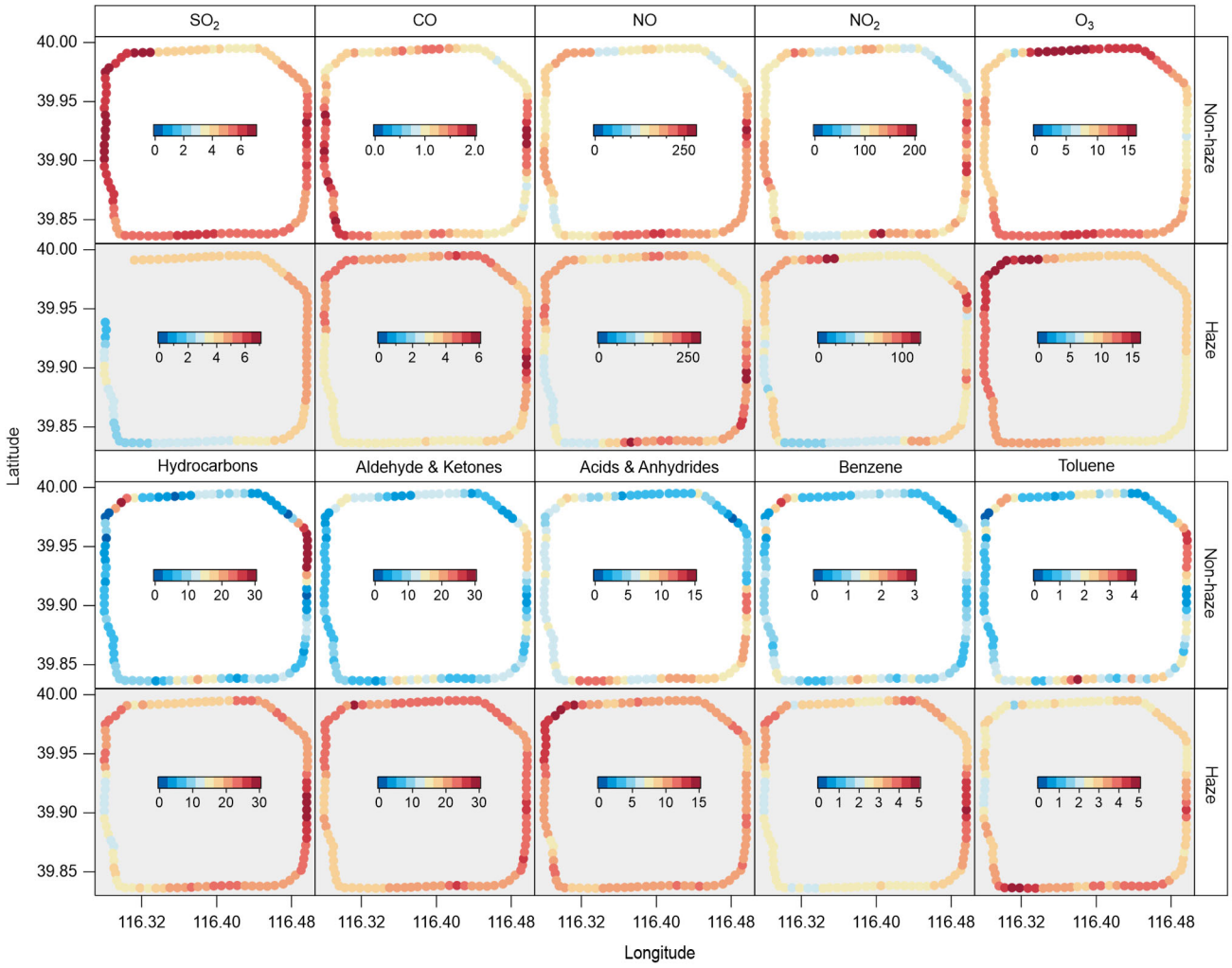

Figure 2. Spatial patterns of the mean mass mixing ratios (Unit: ppmv for CO and ppbv for others) of gas pollutants measured on the 4th Ring Road in Beijing. Data covered from 9 a.m. to 4 p.m. during the measurement period.

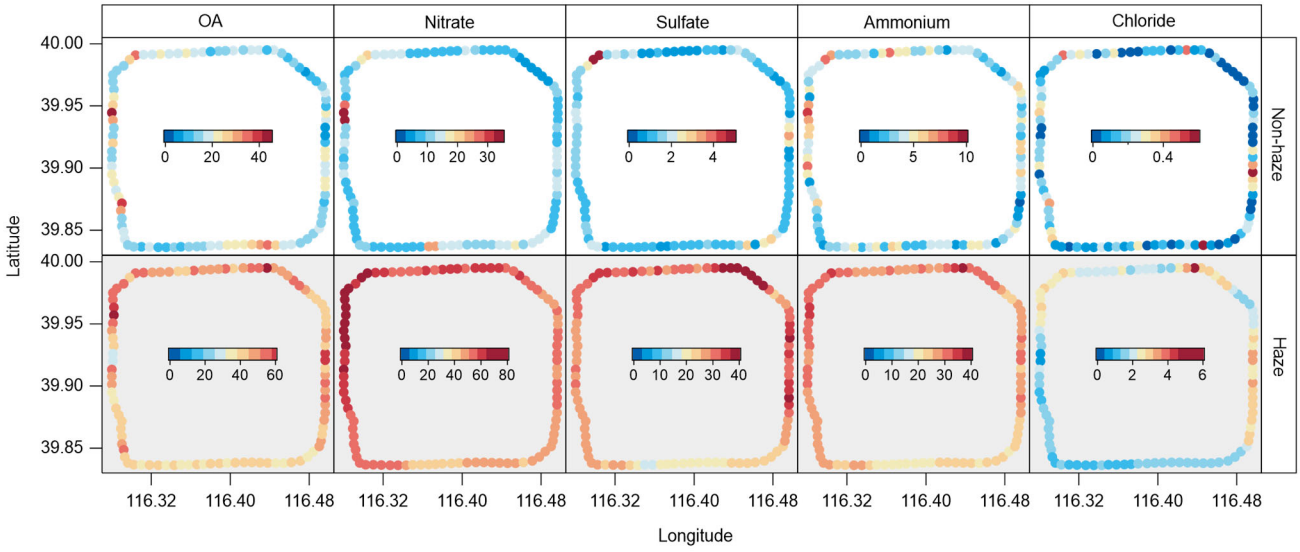
OA
Nitrate
Sulfate
Ammonium
Chloride
Non-haze
Haze
Latitude
Longitude
40.00
39.95
39.90
39.85
116.32
116.40
116.48
0 20 40
0 10 20 30
0 2 4
0 5 10
0 0.4
0 20 40 60
0 20 40 60 80
0 10 20 30 40
0 10 20 30 40
0 2 4 6

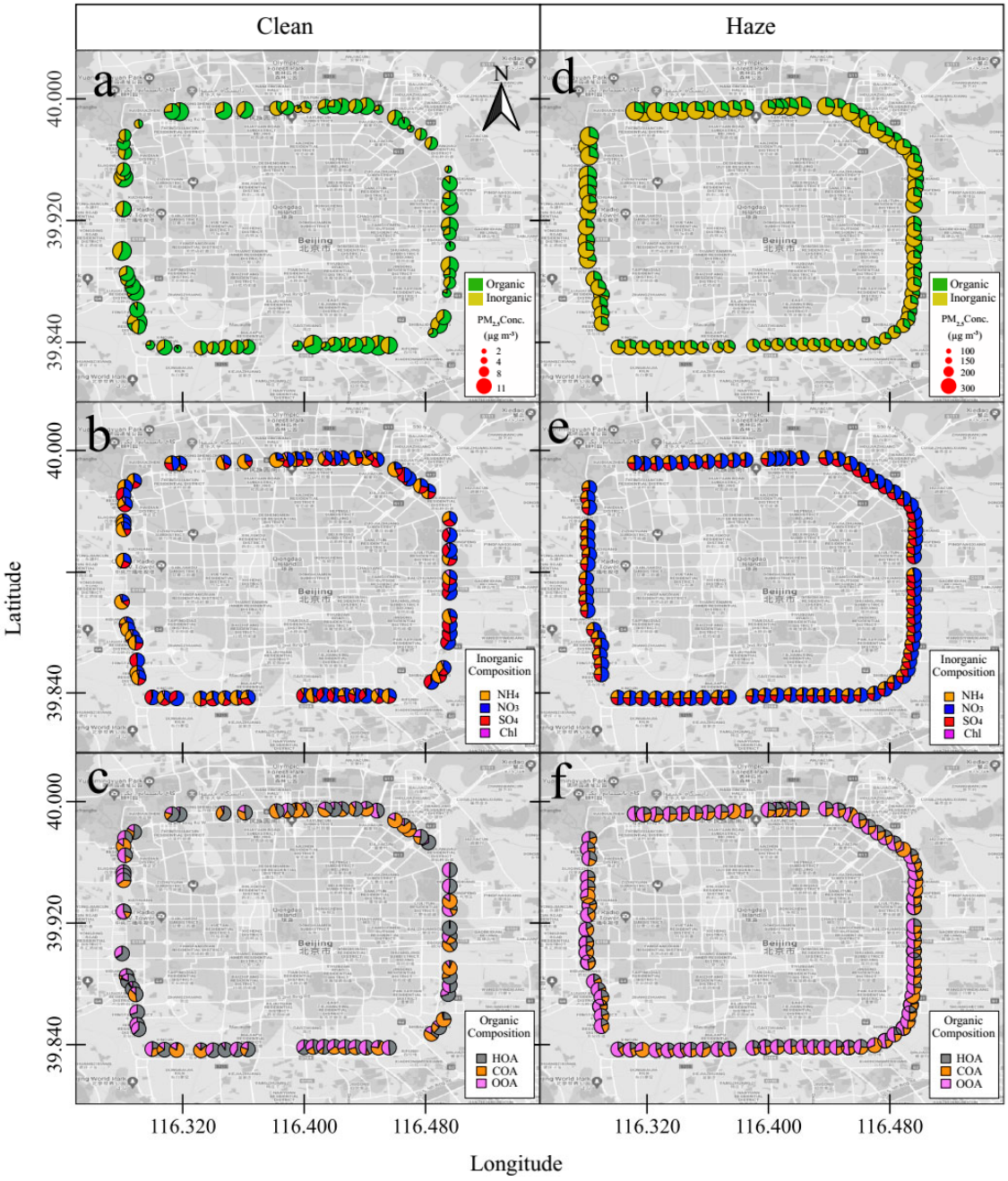

Figure 3. Spatial patterns of the mean mass concentrations (Unit: μg m^{-3}) of the key $PM_{2.5}$ chemical components measured on the 4th Ring Road in Beijing. Data covered from 9 a.m. to 4 p.m. during the measurement period~~**Figure 1.** Spatial distribution of (a, d) the mass concentration (μg m^{-3}), (b, e) the inorganic composition, and (c, f) the organic composition of NR-$PM_{2.5}$ measured during the noon cycles from ~11:00 AM to ~12:30 PM for the clean day on 18 November 2018 and the haze day on~~

~~14 November 2018. The size of the pies for inorganic and organic composition is the same and does not correspond to the mass concentrations of components~~.

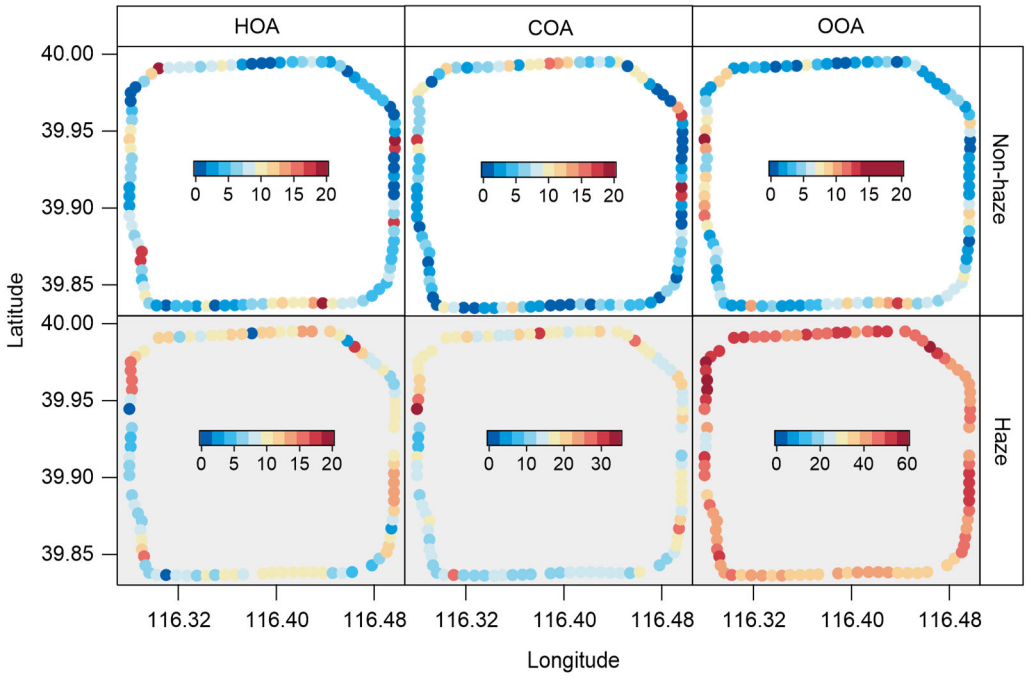

Figure 4. Spatial patterns of the mean mass concentrations (Unit: μg m^{-3}) of OA factors resolved by the PMF analysis of organic mass spectra obtained by the TOF-ACSM on the 4th Ring Road in Beijing. Data covered from 9 a.m. to 4 p.m. during the measurement period.

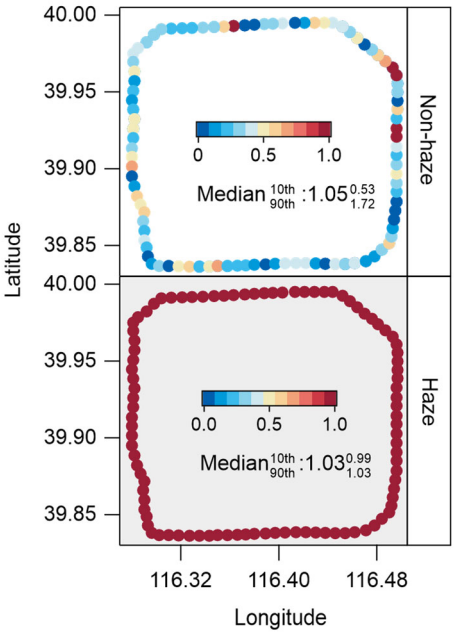

875

Figure 5. Spatial patterns of the molar ratio of $n_{NH_4^+}$: $(2\times n_{SO_4^{2-}} + n_{NO_3^-})$ derived from the aerosol measurements on the 4th Ring Road in Beijing. Data covered from 9 a.m. to 4 p.m. during the measurement period.

~~The organic composition is obtained from the PMF analysis, in which OOA represents the sum of the three OOA factors.~~

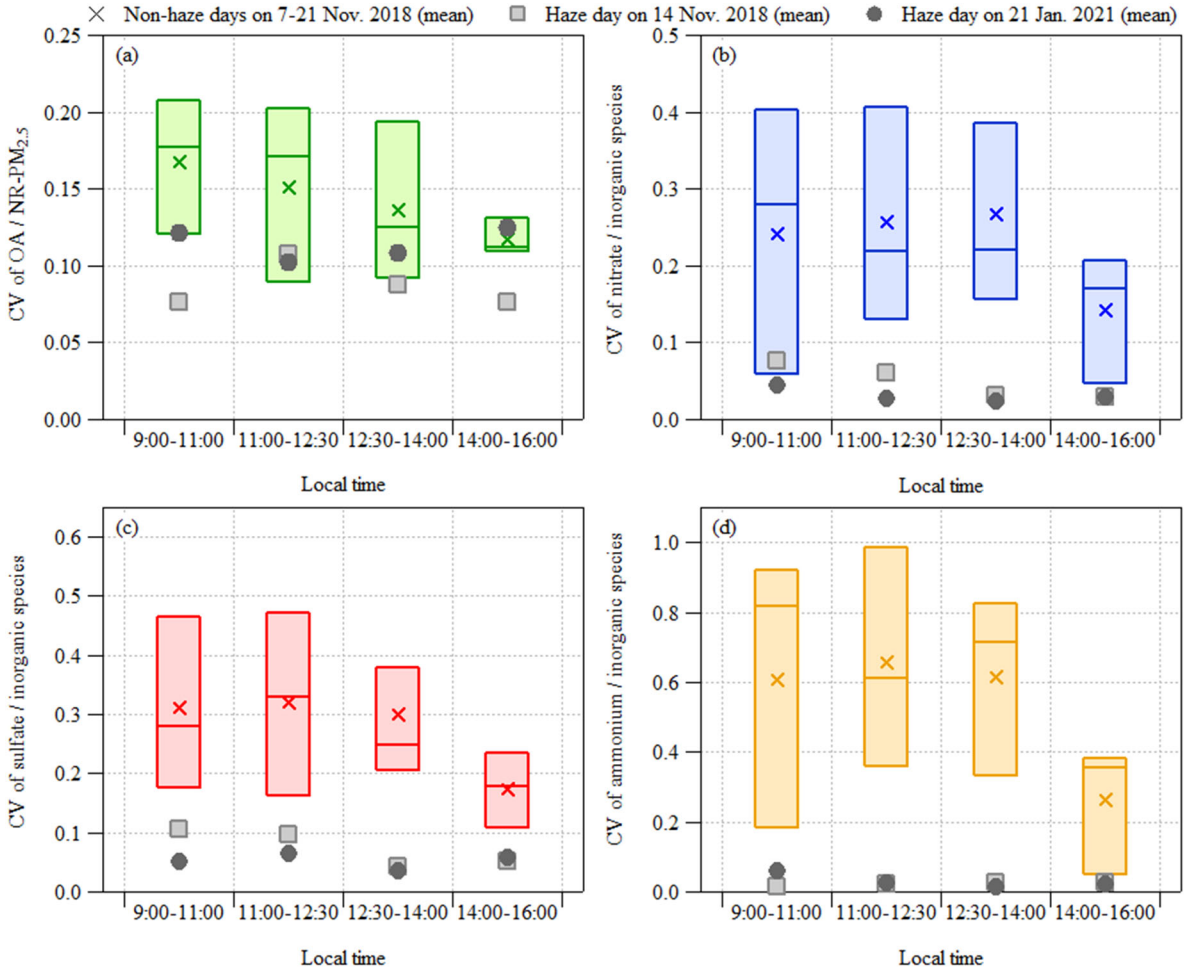

~~Figure 2.~~ ~~The CV values for the inorganic and organic mass fraction in NR-$PM_{2.5}$ for all cycles during the mobile campaign. The box plots show the 75th, median, and 25th percentiles.~~

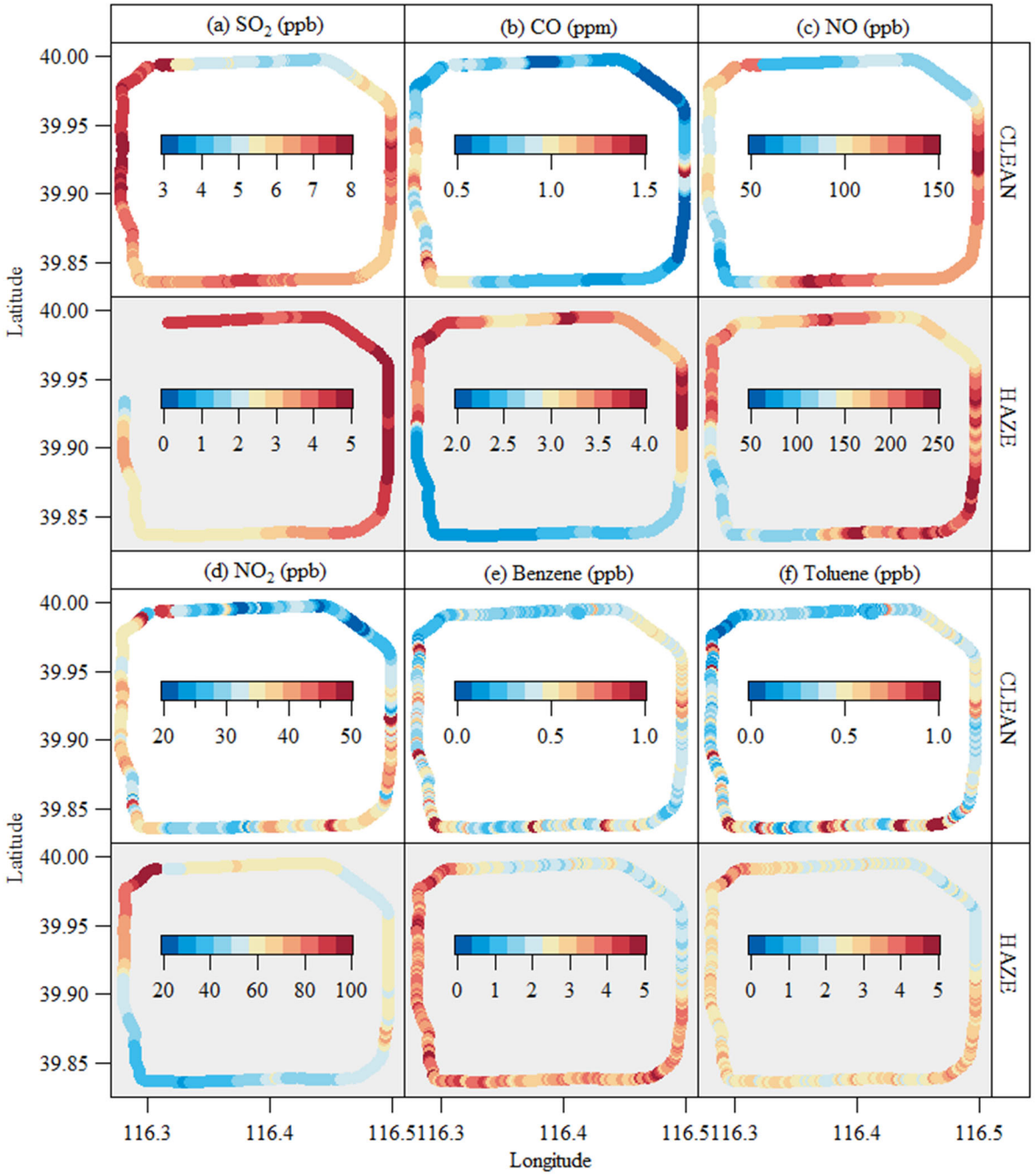

~~**Figure 3.** Spatial distributions of gaseous pollutants including (a) SO_2, (b) CO, (c) NO, (d) NO_2, (e) benzene, and (f) toluene measured during the noon cycles from ~11:00 AM to ~12:30 PM for the clean day on 18 November 2018 and the haze day on 14 November 2018.~~

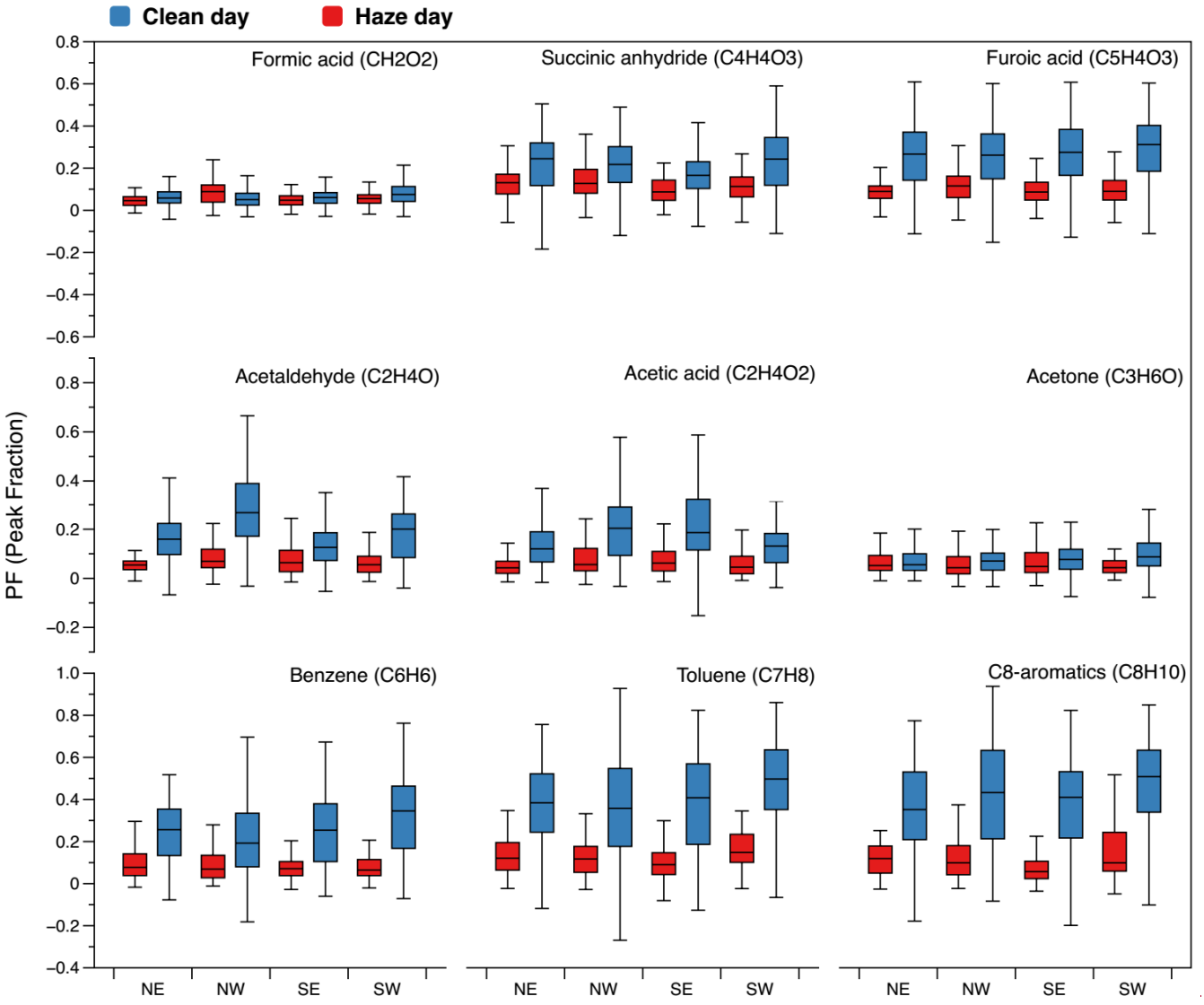
Clean day
Haze day
PF (Peak Fraction)
Formic acid (CH2O2)
Succinic anhydride (C4H4O3)
Furoic acid (C5H4O3)
Acetaldehyde (C2H4O)
Acetic acid (C2H4O2)
Acetone (C3H6O)
Benzene (C6H6)
Toluene (C7H8)
C8-aromatics (C8H10)
NE
NW
SE
SW

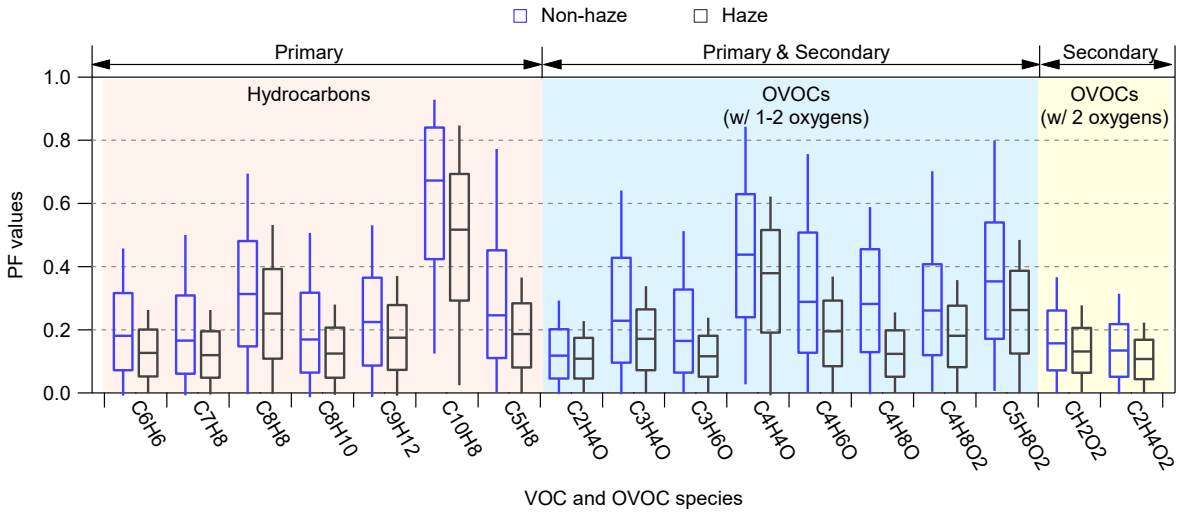

Figure 64. ~~The spatial distributions of p~~Peak fraction (PF) values for common VOC species measured ~~during the noon cycles from ~11:00 AM to ~12:30 PM for the clean day on 18 November 2018 and the haze day on 14 November 2018.~~on the 4th Ring Road in Beijing. Data covered from 9 a.m. to 4 p.m. during the measurement period. The box and whisker plots show the median, 75th and 25th percentiles, and 90th and 10th percentiles of PF values calculated for each data point.

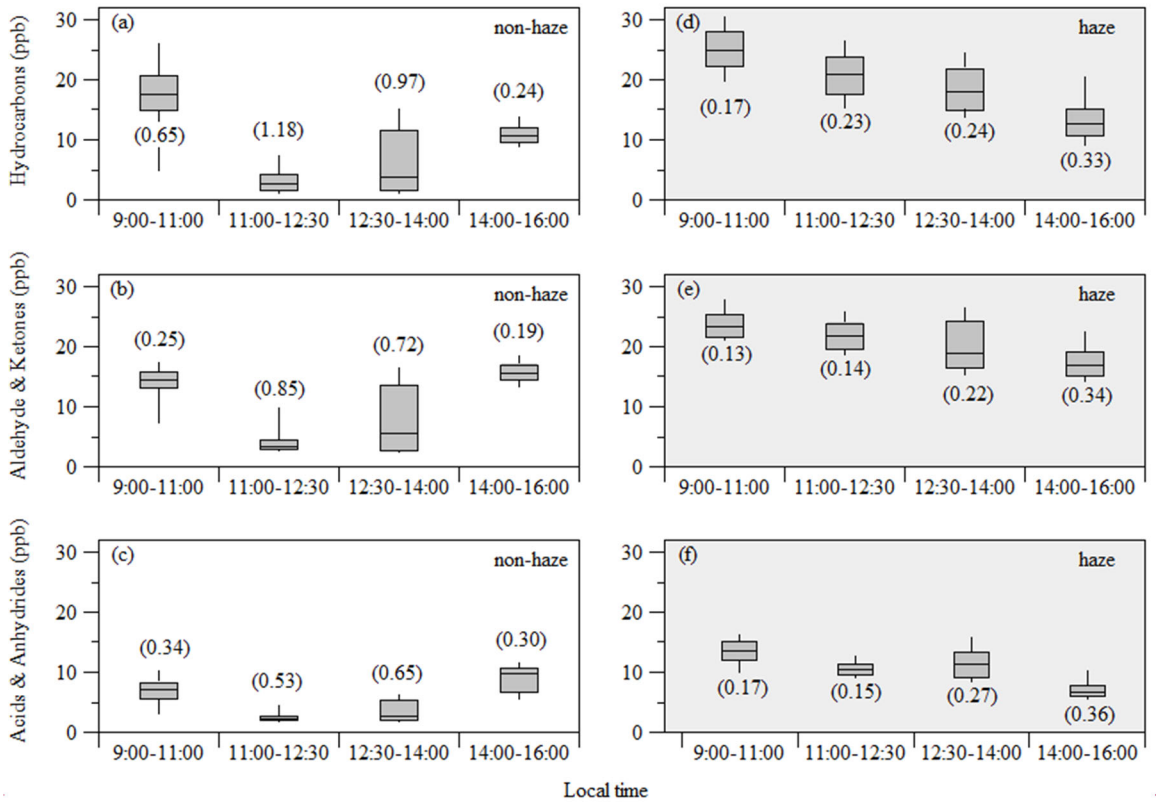
Hydrocarbons (ppb)
Aldehyde & Ketones (ppb)
Acids & Anhydrides (ppb)
(a)
non-haze
(0.65)
(1.18)
(0.97)
(0.24)
(b)
non-haze
(0.25)
(0.85)
(0.72)
(0.19)
(c)
non-haze
(0.34)
(0.53)
(0.65)
(0.30)
(d)
haze
(0.17)
(0.23)
(0.24)
(0.33)
(e)
haze
(0.13)
(0.14)
(0.22)
(0.34)
(f)
haze
(0.17)
(0.15)
(0.27)
(0.36)
0
10
20
30
9:00-11:00
11:00-12:30
12:30-14:00
14:00-16:00
Local time

895

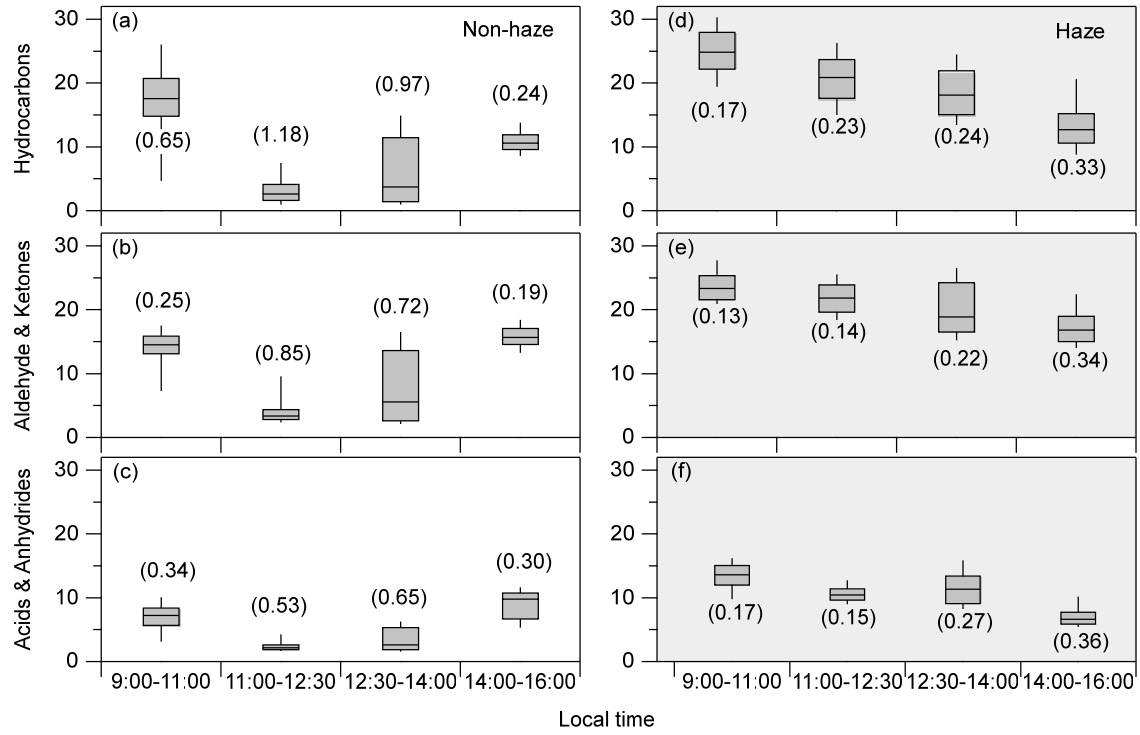

Figure 7~~5~~. Spatial-temporal distributions of the ~~concentrations~~ mixing ratios (Unit: ppbv) of ∑ hydrocarbons, ∑ (aldehydes and ketones), and ∑ (acids and anhydrides) measured during the non-haze and haze days. ~~The numbers in parentheses represent the CV values.~~ The box and whisker plots show median, 75th and 25th percentiles, 90th and 10th percentiles of all data points. The numbers in parentheses represent the CV values. Data covered from 9 a.m. to 4 p.m. during the measurement period.

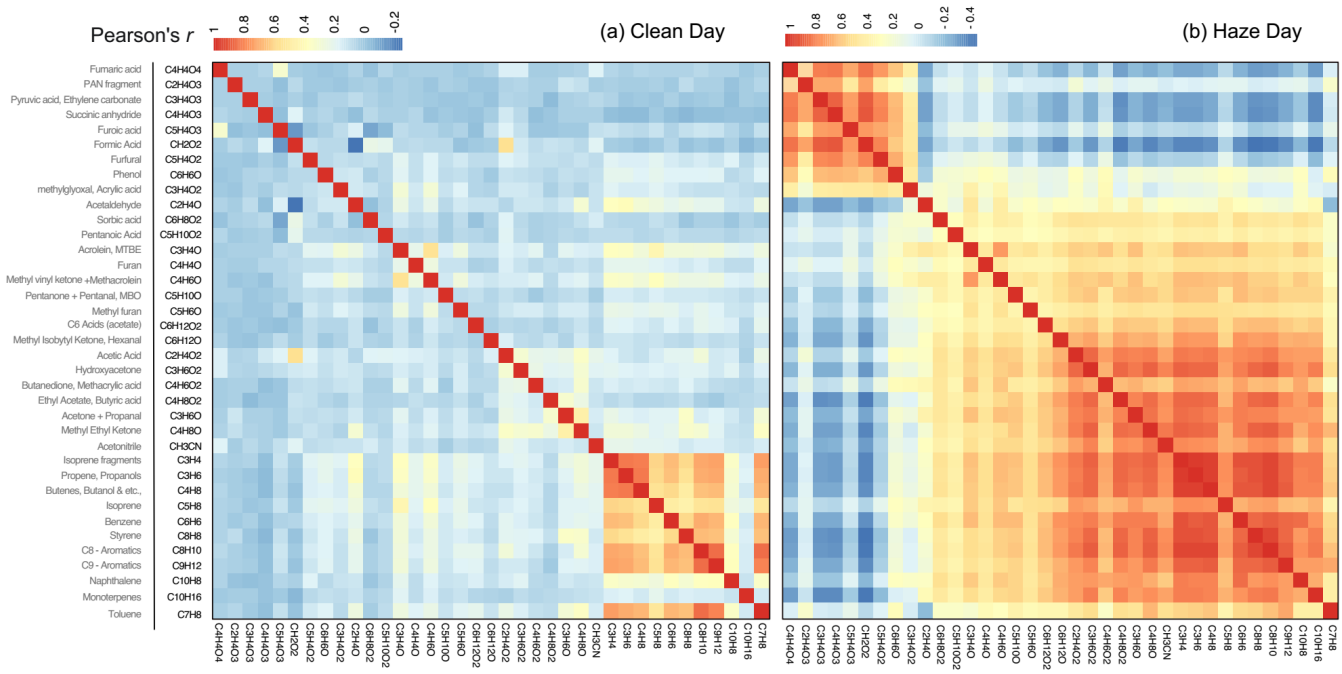

Figure 86. Correlation heatmaps for the concentrations of the main VOCs and OVOCs measured during (a) the clean day on 18 November 2018 and (b) the haze day on 14 November 2018.